

An Excimer to Exciplex Transition through Realization of Donor-Acceptor Interaction in Luminescent Solvent-free Liquid

Vivek Chandrakant Wakchaure,^{a,b} Goudappagouda,^{a,b} Tamal Das,^c Sapna Ravindranathan,^{b,d} Sukumaran Santhosh Babu*^{a,b}

- a. Organic Chemistry Division, National Chemical Laboratory (CSIR-NCL), Pune-411 008, India.
- b. Academy of Scientific and Innovative Research (AcSIR), Ghaziabad-201 002, India.
- c. Physical and Materials Chemistry Division, National Chemical Laboratory (CSIR-NCL), Pune - 411 008, India.
- d. Central NMR Facility, National Chemical Laboratory (CSIR-NCL), Dr. Homi Bhabha Road, Pune - 411008, India.

Table of Contents

| | |
|-------------------|----------|
| 1. Experimental | Page S2 |
| 2. Synthesis | Page S5 |
| 3. Figures S1-S31 | Page S15 |
| 4. Tables S1-S14 | Page S38 |
| 5. References | Page S47 |

1. Experimental

Materials

All chemicals, 12-Tricosanone, 1-Bromo-2-ethylhexane, 1,8-Naphthalic anhydride, hexane-1-amine, 1-bromo hexane, ammonium acetate, sodium cyanoborohydride, dithranol matrix (DT), 2,6-Dihydroxynaphthalene, Hydrochloric acid, 1-methyl-2,4-dinitrobenzene, 1-methyl-4-nitrobenzene, 1-methyl-2-nitrobenzene, nitrobenzene, 4-nitrophenol, toluene, picric acid, anthracene-9,10-dione, benzoquinone, benzene-1,2,4,5-tetracarbonitrile, were purchased from commercial suppliers and used as such without further purification. Solvents such as N, N-dimethylformamide, dichloromethane, methanol, diethyl ether, n-hexane, petroleum ether, ethyl acetate were distilled prior to use.

Thin-layer chromatography was carried out using Aluchrosep Silica Gel 60/UV254 purchased from Merck Specialities Pvt Ltd and visualized either by UV Fluorescence or by iodine chamber. Column chromatography was performed using silica gel (100-200 mesh), the bed was made by using 60-120 mesh silica purchased from Spectrochem Pvt. Ltd. India and mixtures of DCM-PET used for elution were distilled before use.

General

All the reactions were carried out in oven-dried round bottom flasks under an argon atmosphere unless otherwise mentioned. The ^1H , ^{13}C NMR spectra were recorded at Bruker-400 MHz NMR spectrometer instrument. The chemical shift values for ^1H (TMS as internal standard) and ^{13}C NMR are recorded in CDCl_3 . The value of the coupling constant (J) is stated in Hertz (Hz). High-resolution mass spectra (HRMS) were recorded on a Thermo Scientific Q-Exactive, Accela 1250 pump. FT-IR spectra were recorded using Bruker Alpha FT-IR spectrometer and reported in the frequency of absorption (cm^{-1}). UV-Vis absorption spectra were recorded on SHIMADZU UV-3600 plus UV-VIS-NIR spectrophotometer while all emission spectra were performed using PTI Quanta Master™ Steady State Spectrofluorometer. Fluorescence lifetimes were measured by time-correlated single-photon counting (TCSPC), using a spectrofluorometer (Horiba Scientific) and an LED excitation source is 374 nm. The quality of the fit has been judged by fitting parameters such as χ^2 (<1.2) as well as visual inspection of the residuals. DSC Q 10 differential scanning calorimeter connected to Q Series PCA (TA Instruments, USA) was used to determine the phase transition temperatures of the molecule. TGA data were collected in METTLER TOLEDO, TGA/SDTA851 instrument. The rheology experiment was carried out using an

MCR dynamic oscillatory Cup and Bob Frequency Sweep at 20 °C by using about 5 ml of the liquid samples. Luminescence quantum yield was measured using a Quanta-Phi 6" model F-3029.

Details of DFT Calculations

All the geometry optimization in this study has been performed with density functional theory (DFT), with the aid of the Turbomole 7.1 suite of programs,^{S1} using the PBE functional.^{S2} The TZVP^{S3} basis set has been employed. The resolution of identity (RI),^{S4} along with the multipole accelerated resolution of identity (marij)^{S5} approximations, have been employed for an accurate and efficient treatment of the electronic Coulomb term in the DFT calculations. Dispersion correction (disp3) was incorporated with optimization calculations. Harmonic frequency calculations were performed for all stationary points to confirm them as a local minima. The single point energy calculation of all the PBE/TZVP optimized compounds has been performed with B3LYP/6-311+G(d) level of theory using Gaussian09^{S6} software packages.

Preparation of liquid exciplex

The molecule **D1** and **N1** with varying equivalents in glass vials (1.5 mL) were either stirred well with a spatula or heated gently to become a homogeneous mixture.

UV VIS spectrum of neat liquids

UV Vis spectra of all neat liquids were recorded in the transmittance mode, and the samples are prepared by making a uniform, transparent coating of 5 mg sample on 1 x 1 cm² area of quartz plate. The consistency of each spectrum was confirmed by repeated trails.

Whatman filter paper strips

A uniform coating on Whatman Filter paper strips was made from 1mM solution of the compounds in dichloromethane.

NMR experiments

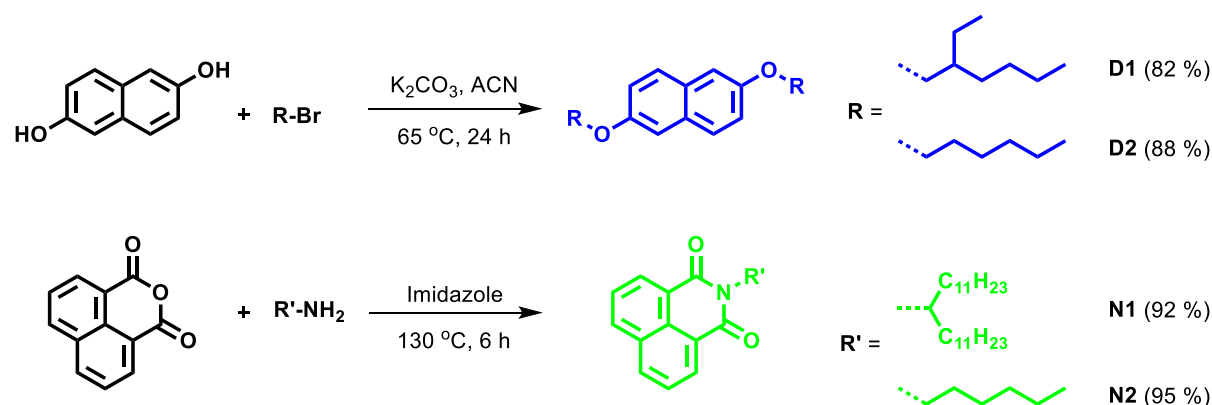
All the NMR spectra in the neat condition (**D1**, **N1** and **D1+N1** exciplex liquids) were recorded by placing the compounds (~ 200 mg) in a 3 mm NMR tube and inserting it in an outer 5 mm NMR tube containing *DMSO-d₆* as an external lock. After mixing, samples were

allowed to homogenize at the measurement temperature before carrying out the experiments. The actual ratios of **D1** and **N1** were estimated by integration of peak areas of the aromatic protons.

Detection of TNT in weight % by using exciplex liquid

A solution was prepared by dissolving TNT in diethyl ether at room temperature and used as a stock solution. The Exciplex liquid with TNT weight % samples spotted (5 mg sample on 1 x 1 cm² area) on a quartz plate. The visible color change is identified by bare eyes, and the fluorescence quenching was monitored under 365 nm illumination by an independent observer. The minimum detection level of TNT was qualitatively judged by the naked eye detectable fluorescence quenching on the glass and quantitatively determined by measuring the fluorescence quenching (%) using the front face technique.

2. Synthesis

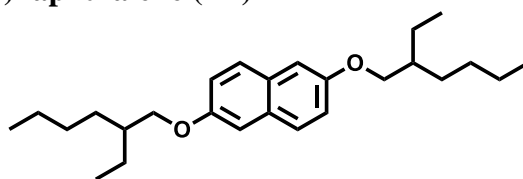


Scheme S1. Synthesis of **D1**, **D2**, **N1**, and **N2**.

General procedure for the synthesis of dialkoxy naphthalene (DAN)^{S7}

Potassium carbonates (5 eq.) was suspended in 50 ml of acetonitrile and was sonicated for 30 min then degassed using N₂ for 30 minutes. Alkyl bromide (5 eq.) was then added. After this, 1,5-dihydroxynaphthalene (1 eq.) suspended in sonicated acetonitrile and added via a dropping funnel. The reaction was then refluxed under N₂ for 24h. The reaction mixture is then filtered through celite pad, the filtrate collected and the solvent removed under reduced pressure. The residue is then dissolved in dichloromethane and washed with 1M HCl, water, brine. The organic layer is then dried over sodium sulfate. The solvent was removed under reduced pressure and the crude product was purified by silica gel column chromatography.

2,6-bis((2-ethylhexyl)oxy)naphthalene (**D1**)



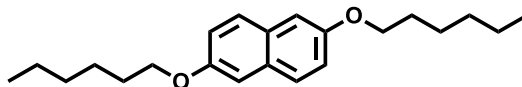
Nature and Yield: colorless liquid, 82%.

¹H-NMR: (400 MHz, CDCl₃, 25 °C): δ = 7.63 (2H, d, J = 8.7 Hz), 7.14-7.12 (2H, dd, J = 8.7 and 2.26 Hz), 7.10 (2H, d, J = 2.26 Hz), 3.95-3.93 (4H, m), 1.79 (2H, m), 1.55-1.38 (8H, m), 1.37-1.34 (8H, m), 0.98-0.91 (12H, m) ppm.

¹³C-NMR: (100 MHz, CDCl₃, 25 °C): δ = 155.7, 129.6, 127.9, 119.2, 106.8, 70.5, 39.4, 30.6, 29.1, 23.9, 23.1, 22.9, 14.1, 11.1 ppm.

HRMS: calcd. for C₂₆H₄₀O₂⁺ = 384.3028, found 384.3023.

2,6-bis(hexyloxy)naphthalene (D2)



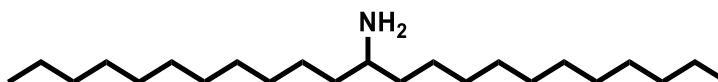
Nature and Yield: solid, 88%.

¹H-NMR: (400 MHz, CDCl₃, 25 °C): δ = 7.64 (2H, d, J = 9.08 Hz), 7.15-7.12 (2H, dd, J = 9.08 and 2.42 Hz), 7.10 (2H, d, J = 2.42 Hz), 4.05 (4H, t, J = 6.65 Hz), 1.88-1.81 (4H, m), 1.55-1.50 (4H, m), 1.40-1.36 (8H, m), 0.94 (6H, t, J = 7.23 Hz) ppm.

¹³C-NMR: (100 MHz, CDCl₃, 25 °C): δ = 155.5, 129.6, 127.9, 119.1, 106.9, 68.1, 31.6, 29.2, 25.8, 22.6, 14.1 ppm.

HRMS: calcd. for C₂₆H₄₀O₂⁺ = 328.2402, found 328.2397.

Tricosan-12-amine^{S8}

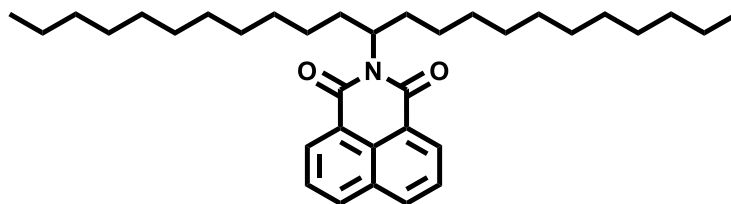


1,2-Tricosanone, NH₄OAc and NaBH₃CN were dissolved in 40 ml methanol (HPLC grade) and stirred at RT for 56 h (3 days). Then the reaction was quenched by adding con. HCl dropwise. The solution was then concentrated with the rotatory evaporator. The solid thus obtained is dispersed in 250 ml of water and adjusted to pH = 10 with KOH. The obtained latex solution was evaporated by 150 ml of CH₂Cl₂ and then 100 ml again. The pale yellow oil was obtained by concentrating the CH₂Cl₂ solution and used as such for the next step without further purification.

General procedure for the synthesis of naphthalenemonoimide (NMI)^{S9}

Amine (1.05 eq.) and 1,8-naphthalic anhydride (1 eq.) were heated in imidazole (10 g) for 6 hours at 130 °C, subsequently cooled, and while still warm combined with a 2 M HCl followed by extraction with DCM twice. The combined organic phases were dried with (Na₂SO₄), the solvent was removed by vacuum, and the product was purified by column chromatography.

2-(tricosan-12-yl)-1H-benzo[de]isoquinoline-1,3(2H)-dione (N1)



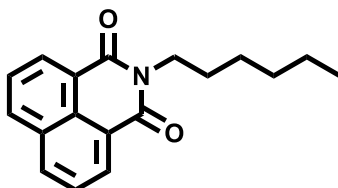
Nature and Yield: pale yellow liquid, 92%.

¹H NMR: (CDCl₃, 400 MHz, 25 °C): δ = 8.60-8.57 (2H, m), 8.19 (2H, d, J = 8.3 Hz), 7.76 (2H, t, J = 8.3 Hz), 5.25-5.13 (1H, m), 2.30-2.15 (2H, m), 1.91-1.75 (2H, m), 1.28-1.20 (36H, m), 0.86 (6H, t, J = 6.18 Hz) ppm.

¹³C NMR: (CDCl₃, 100 MHz, 25.0 °C): δ = 165.4, 164.3, 133.5, 131.5, 131.5, 130.8, 128.3, 126.9, 123.4, 123.7, 54.4, 32.4, 31.8, 29.5, 29.5, 29.2, 26.9, 22.6, 14.1 ppm.

HRMS: calcd. for C₃₅H₅₃NO₂⁺ = 519.4076, found 519.4071.

2-hexyl-1H-benzo[de]isoquinoline-1,3(2H)-dione (N2)

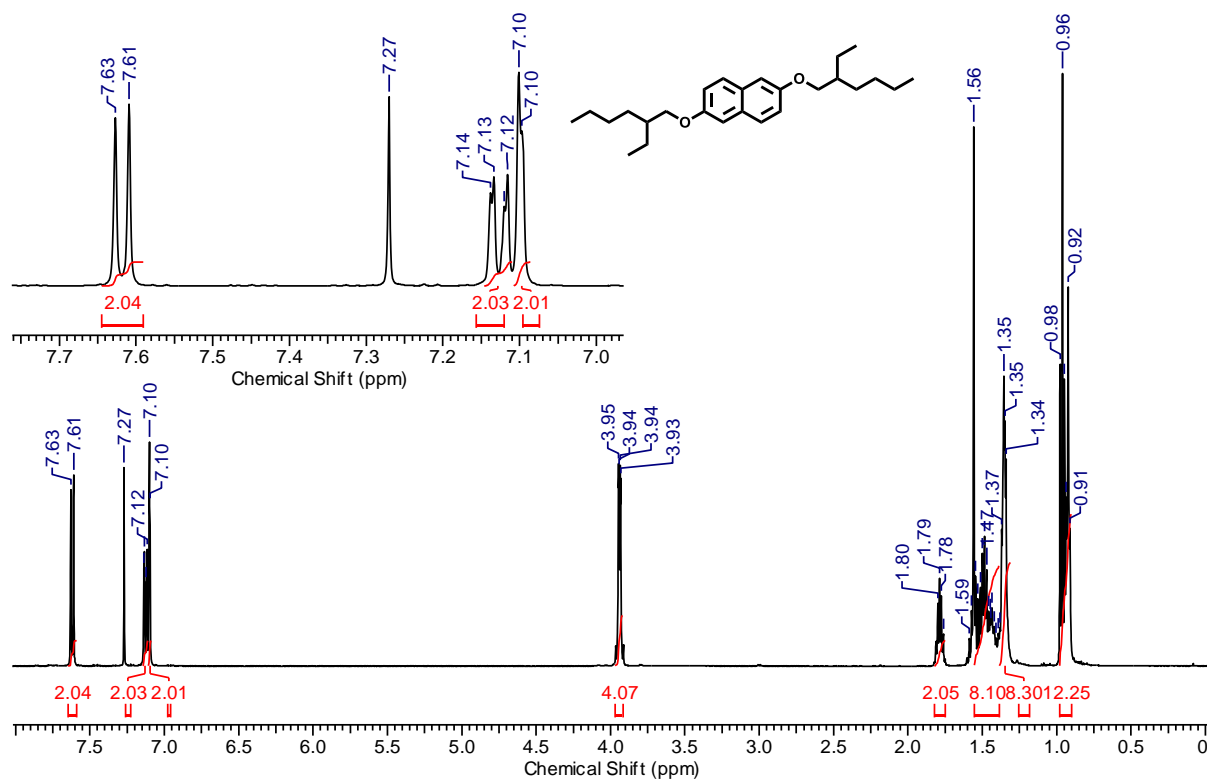


Nature and Yield: pale yellow solid, 95%.

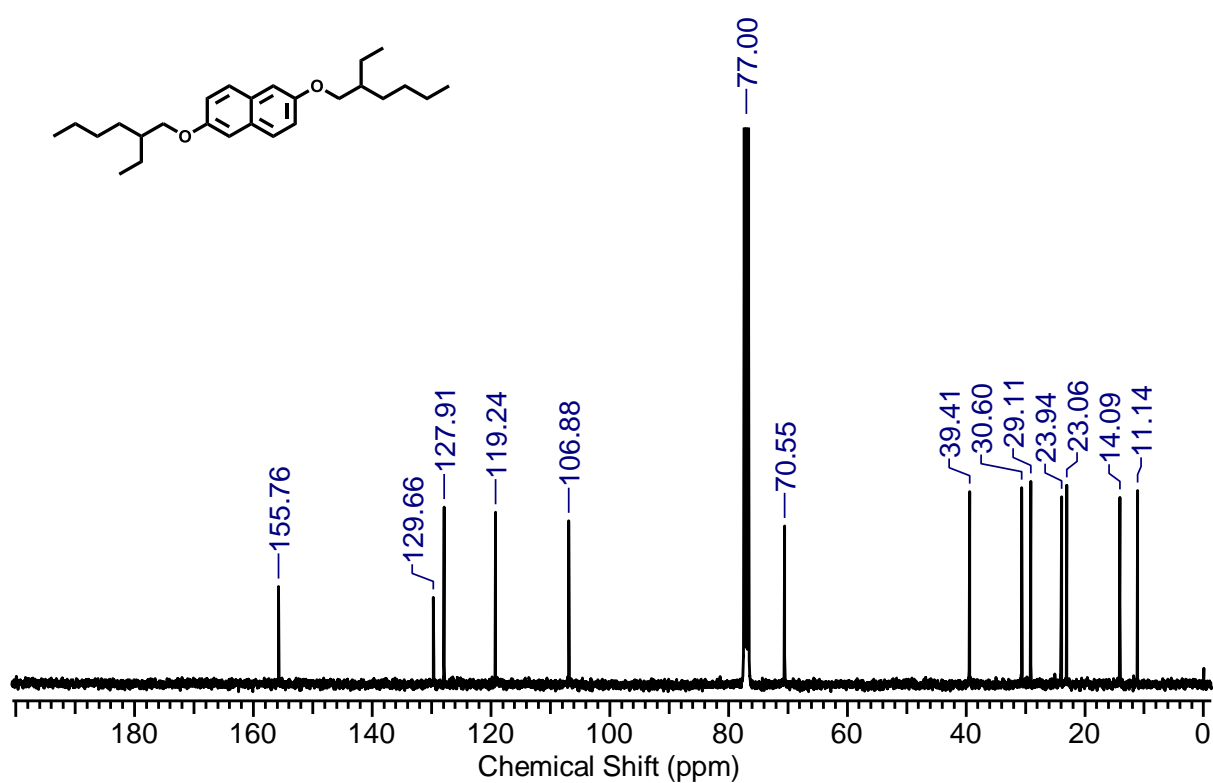
¹H NMR: (CDCl₃, 400 MHz, 25 °C): δ = 8.61-8.59 (2H, m), 8.21 (2H, d, J = 8.03), 7.75 (2H, t, J = 8.03 Hz), 4.18 (2H, t, J = 7.62 Hz), 1.77-1.70 (2H, m), 1.45-1.40 (2H, m), 1.37-1.32 (4H, m), 0.89 (3H, t, J = 7.17 Hz) ppm.

¹³C NMR: (CDCl₃, 100 MHz, 25.0 °C): δ = 164.2, 133.8, 131.5, 131.1, 128.1, 126.9, 122.7, 40.5, 31.5, 28.1, 26.7, 22.6, 14.0 ppm.

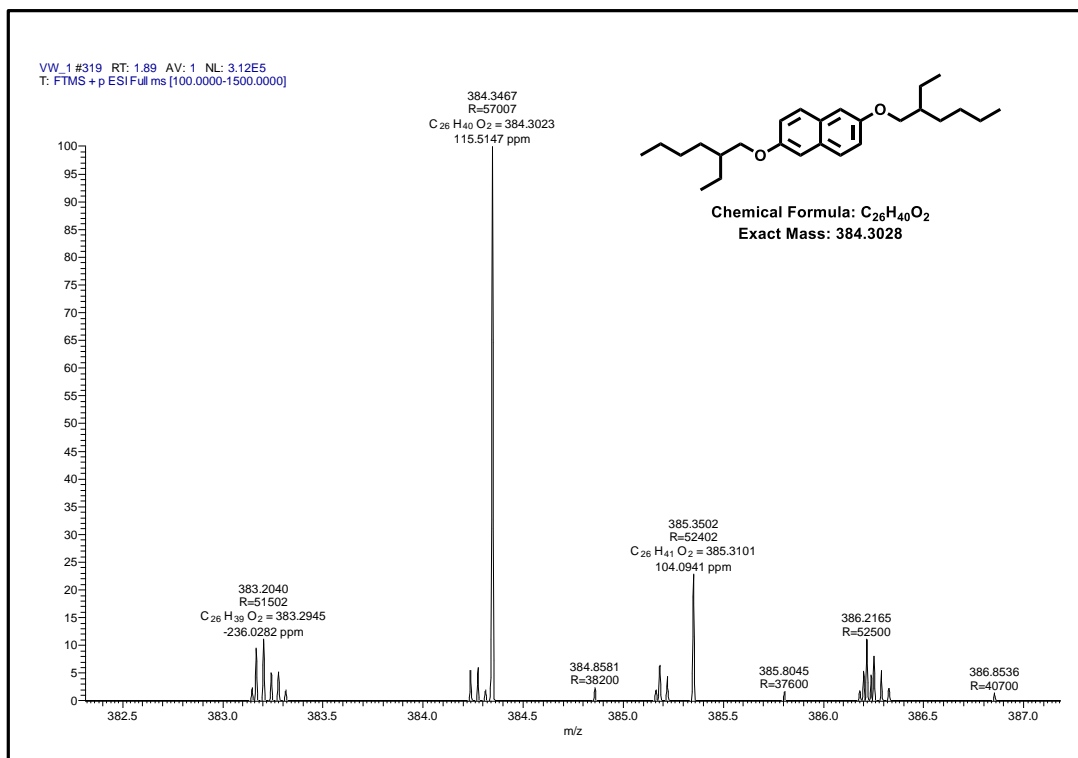
HRMS: calcd. for C₁₈H₂₀NO₂⁺ = 282.1416, found 282.1489.



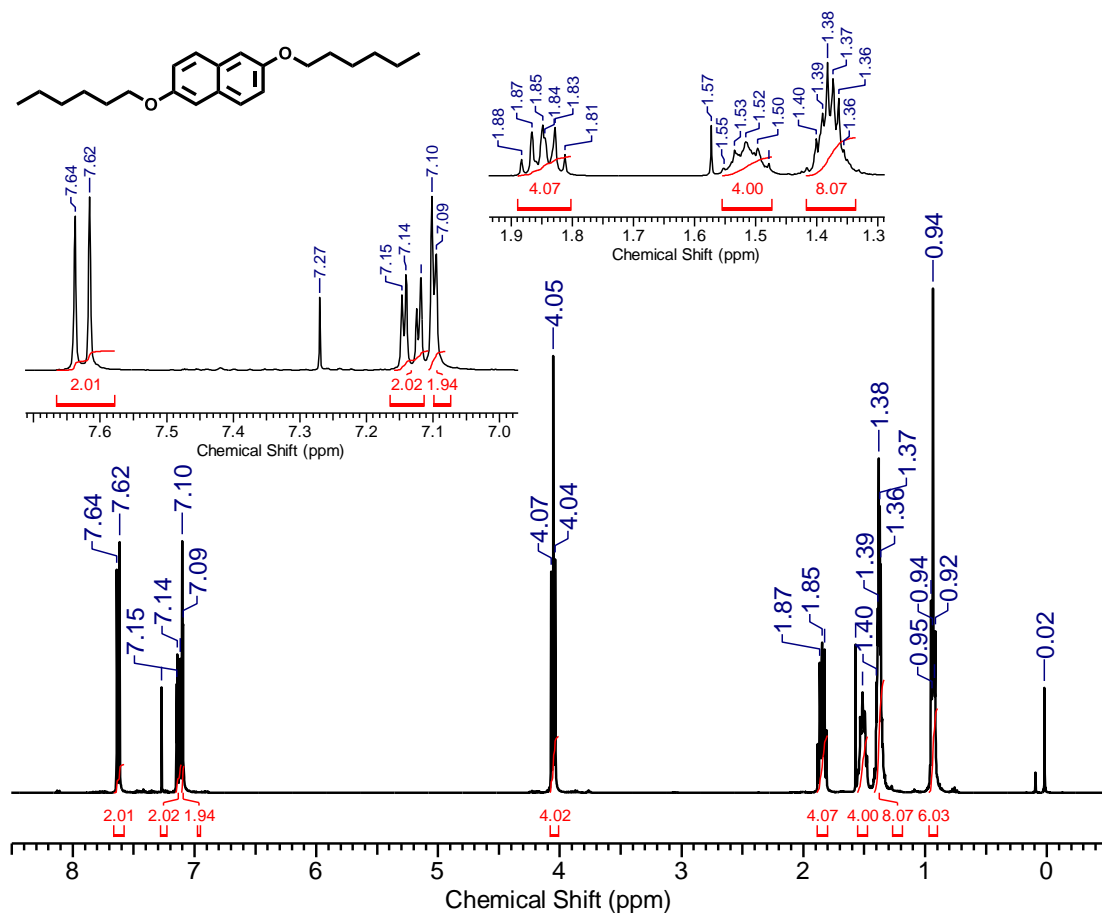
^1H NMR spectra of 2,6-bis((2-ethylhexyl)oxy)naphthalene (**D1**).



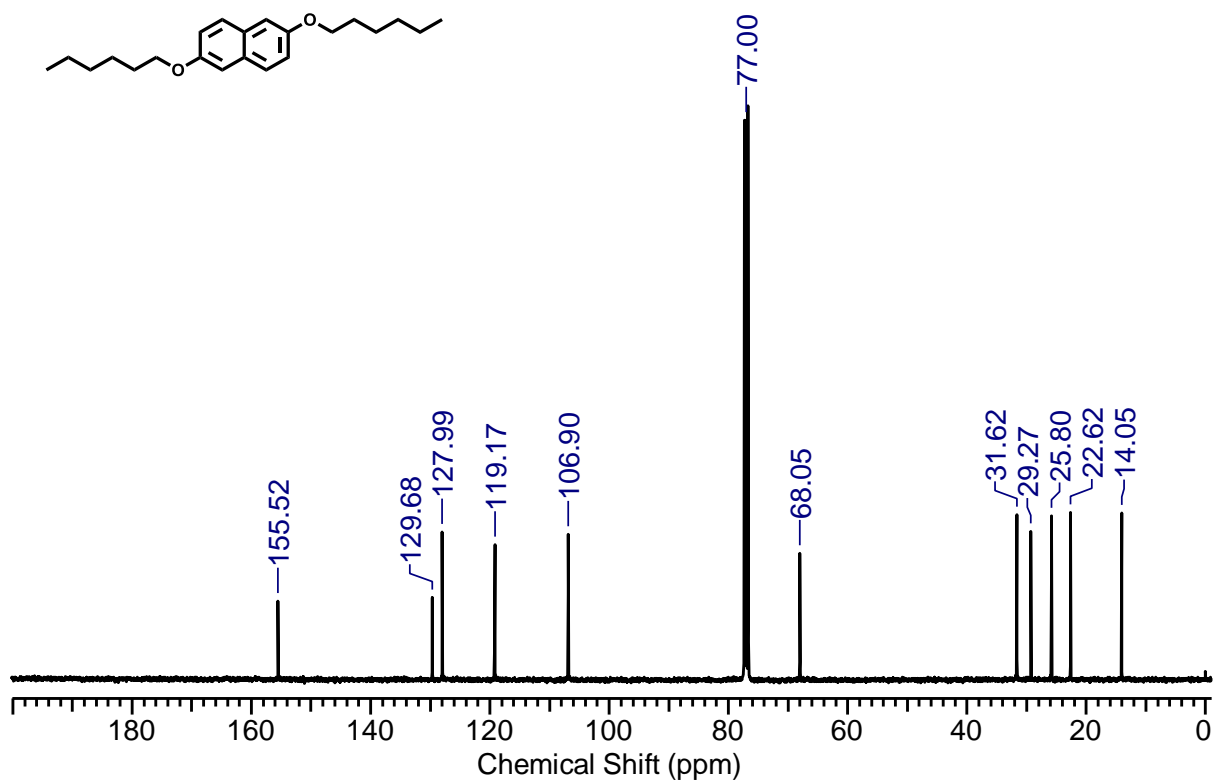
^{13}C NMR spectra of 2,6-bis((2-ethylhexyl)oxy)naphthalene (**D1**).



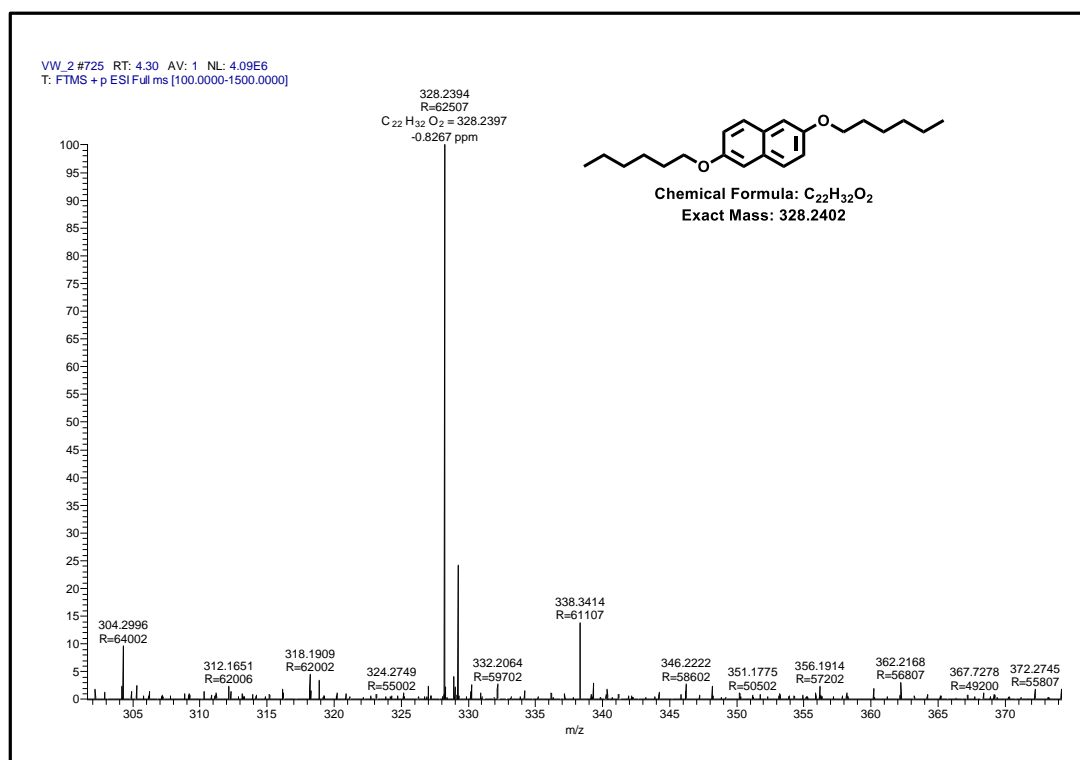
HRMS of 2,6-bis((2-ethylhexyl)oxy)naphthalene (**D1**).



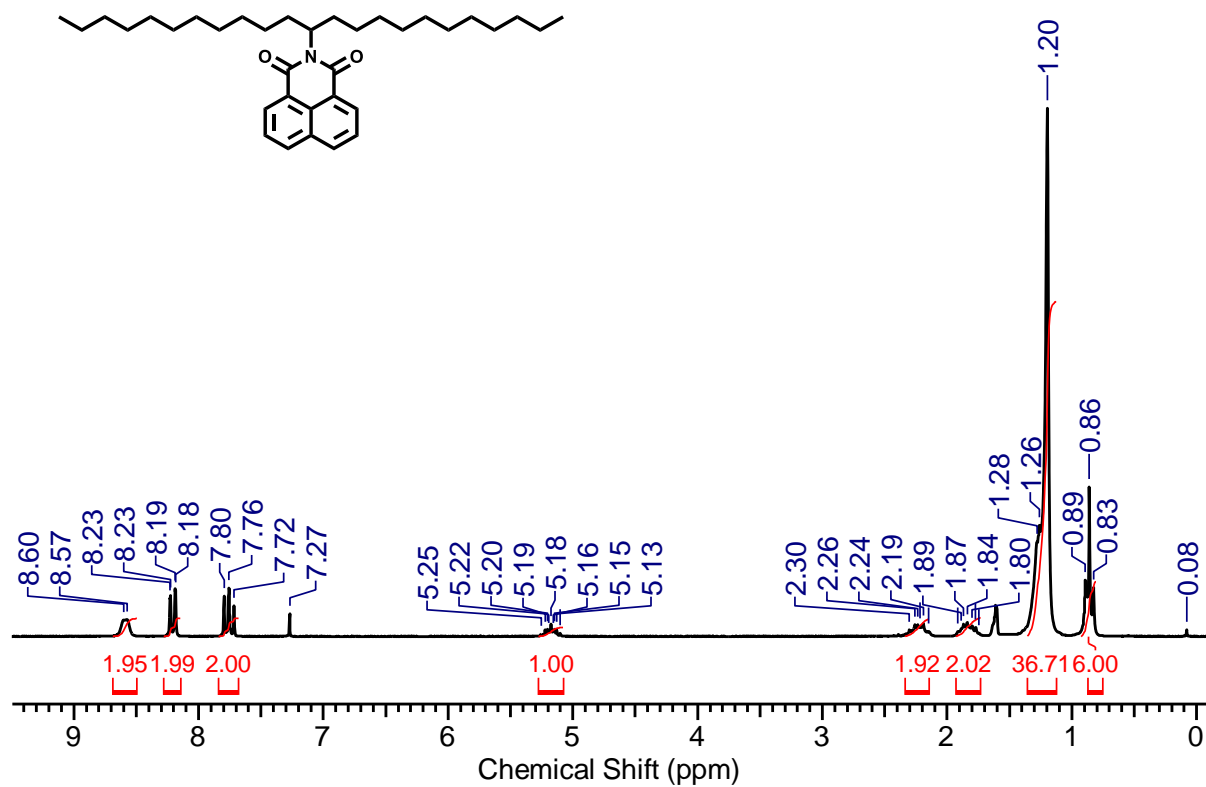
1H NMR spectra of 2,6-bis(hexyloxy)naphthalene (**D2**).



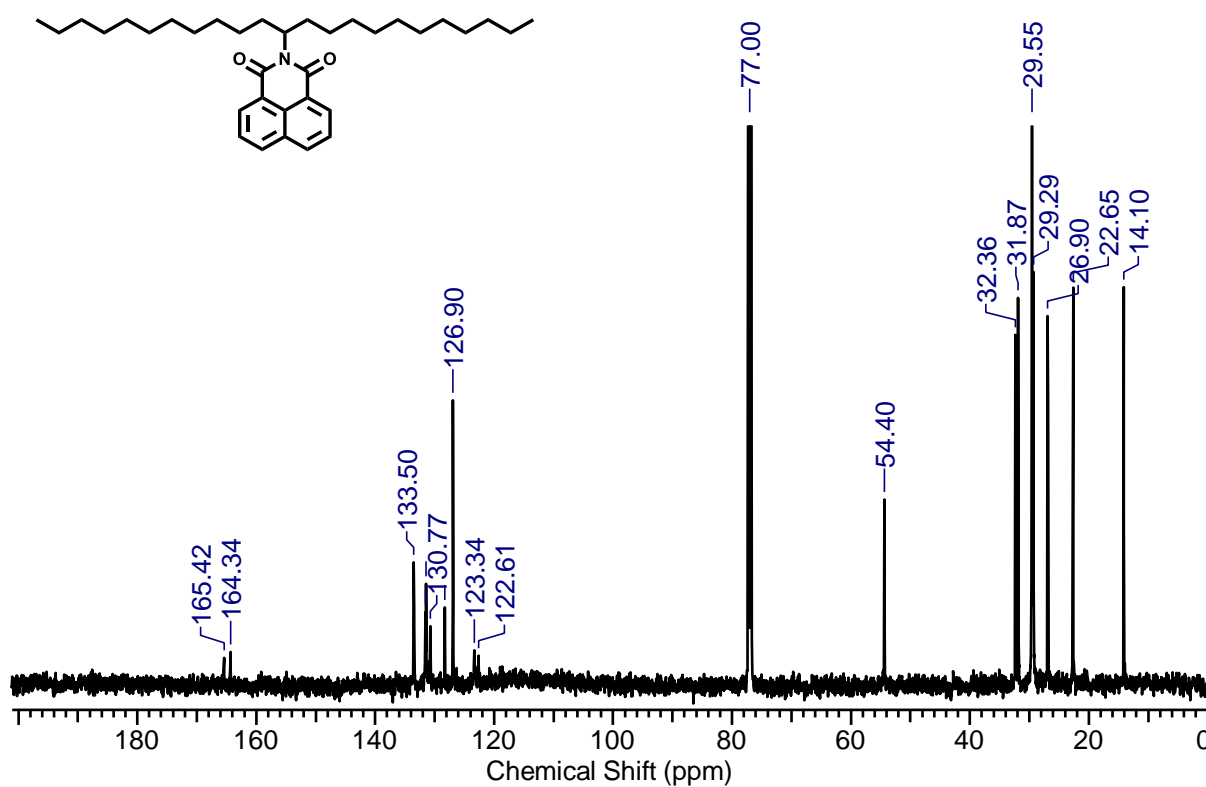
¹³C NMR spectra of 2,6-bis(hexyloxy)naphthalene (D2).



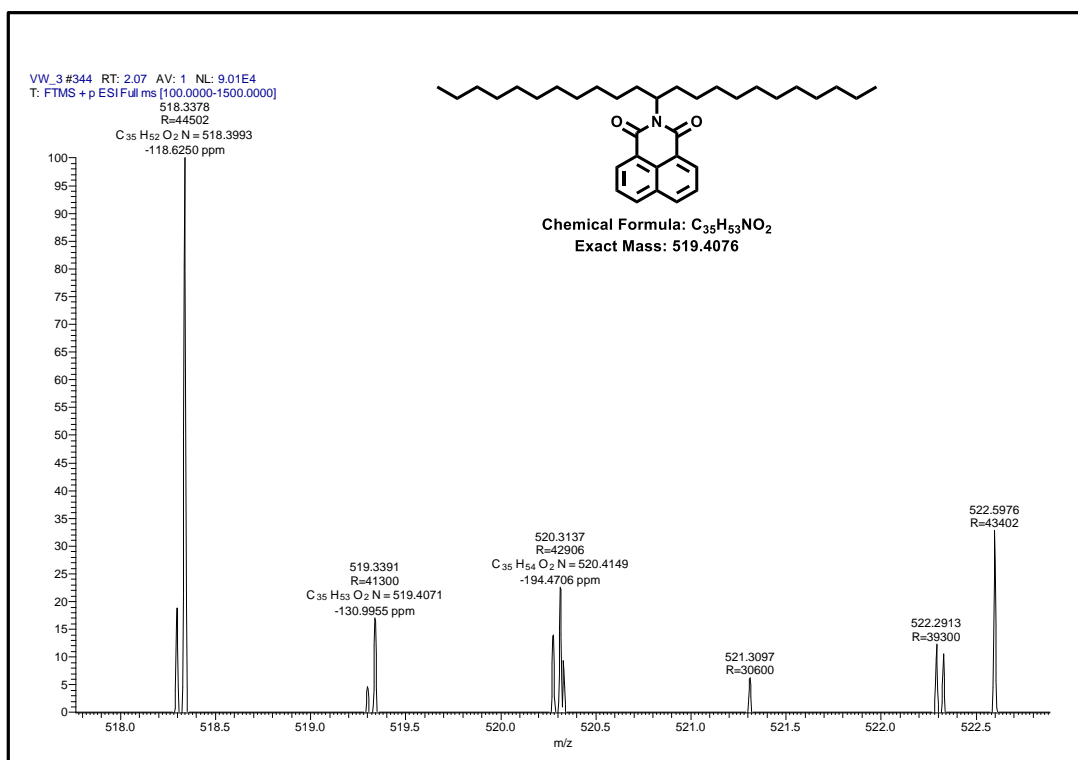
HRMS of 2,6-bis(hexyloxy)naphthalene (D2).



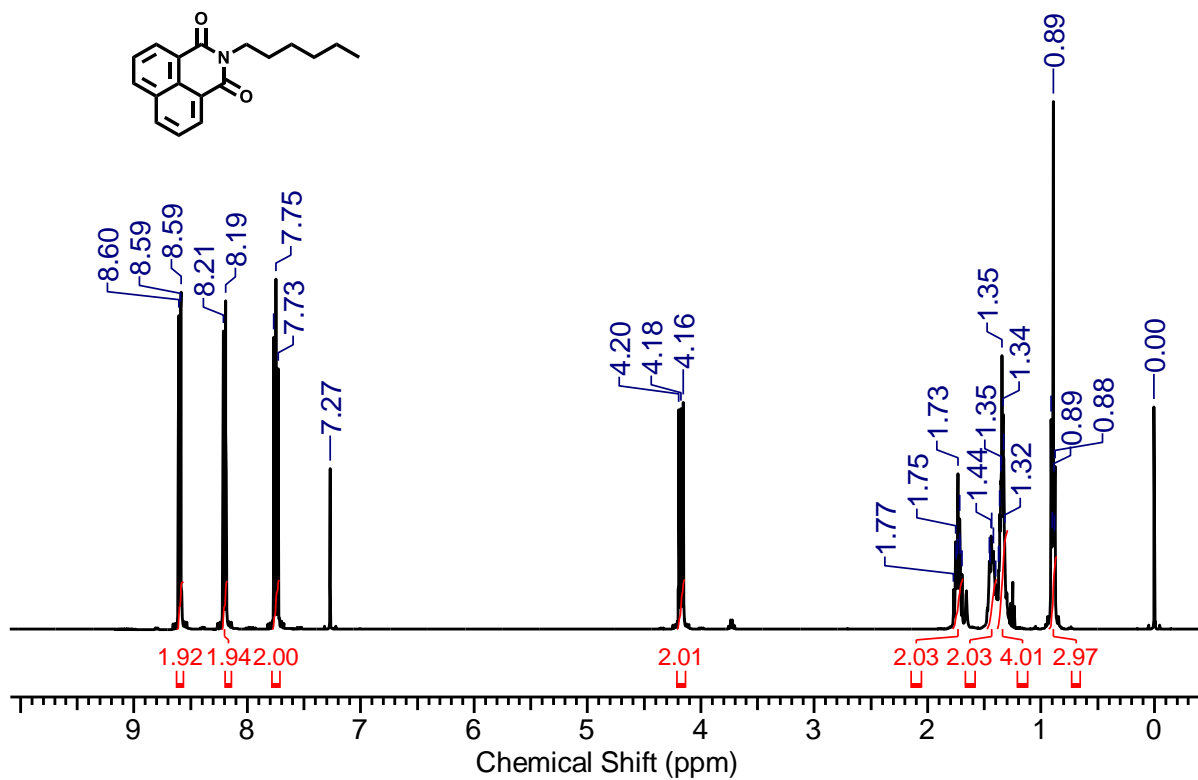
¹H NMR spectra of 2-(tricosan-12-yl)-1H-benzo[de]isoquinoline-1,3(2H)-dione (N1).



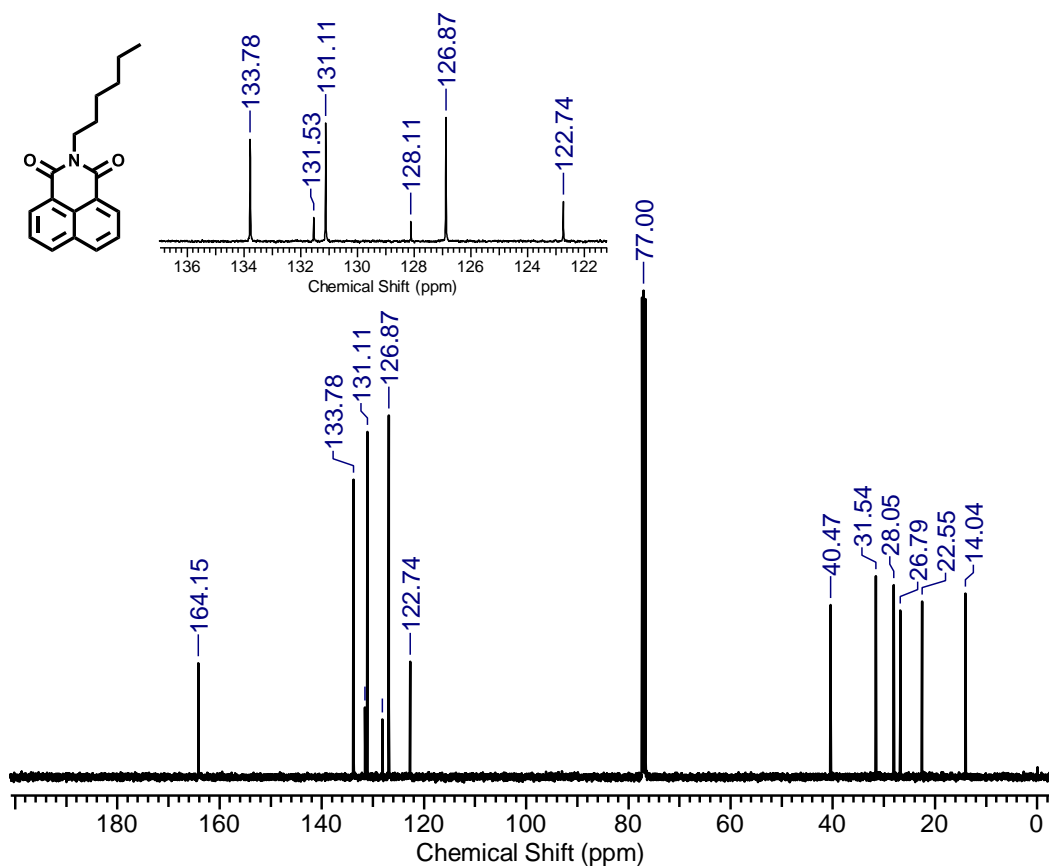
¹³C NMR spectra of 2-(tricosan-12-yl)-1H-benzo[de]isoquinoline-1,3(2H)-dione (N1).



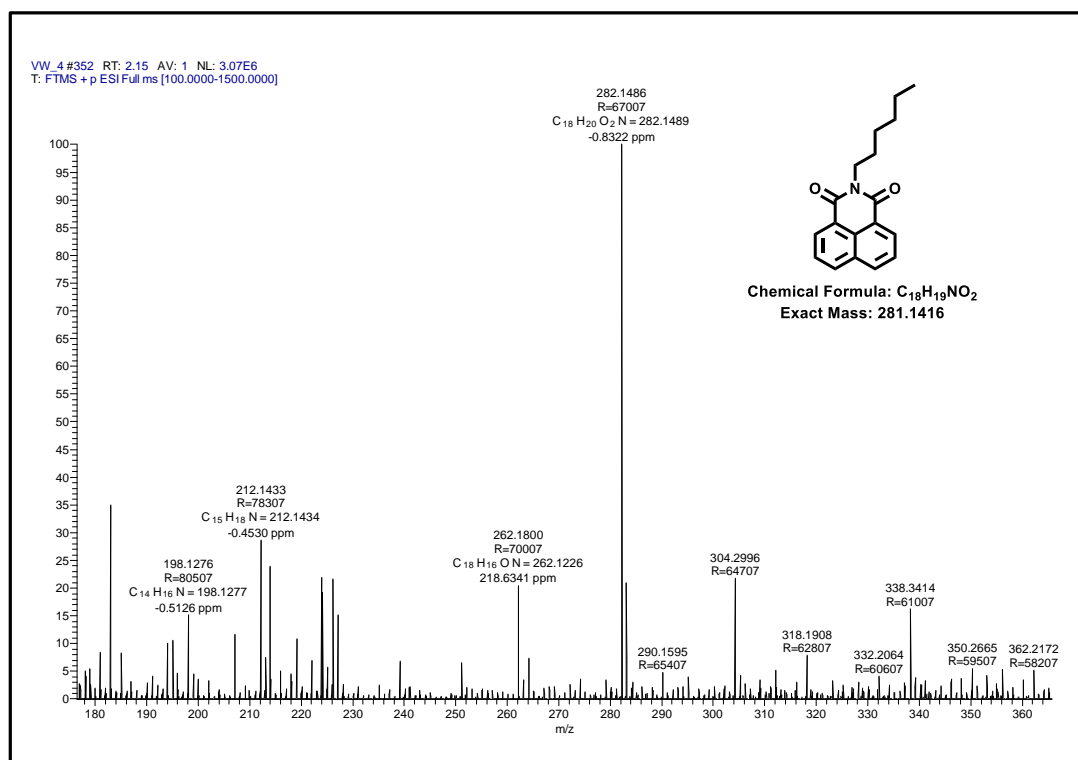
HRMS of 2-(tricosan-12-yl)-1H-benzo[de]isoquinoline-1,3(2H)-dione (N1).



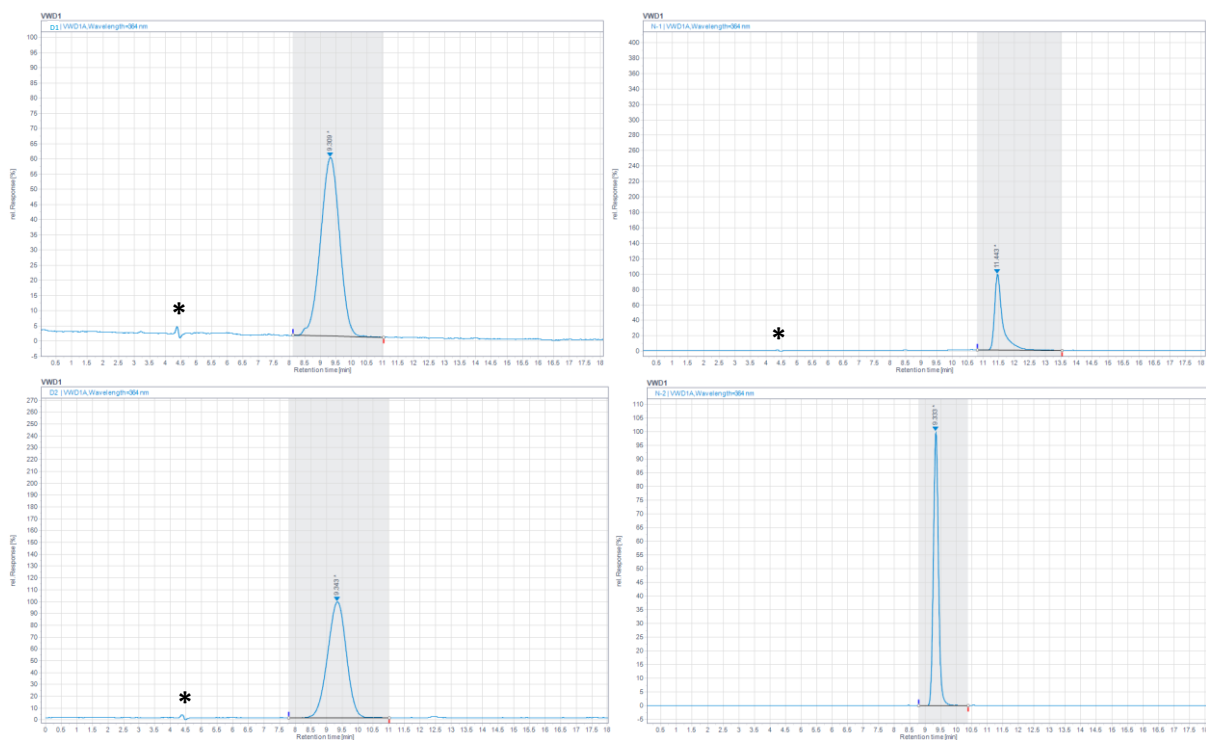
¹H NMR spectra of 2-hexyl-1H-benzo[de]isoquinoline-1,3(2H)-dione (N2).



¹³C NMR spectra of 2-hexyl-1H-benzo[de]isoquinoline-1,3(2H)-dione (N2).



HRMS of 2-hexyl-1H-benzo[de]isoquinoline-1,3(2H)-dione (N2).



HPLC profile of **D1** (RT = 9.309), **D2** (RT = 9.343), **N1** (RT = 11.443) and **N2** (RT = 9.333) in acetonitrile:H₂O (90:10) by monitoring at 364 nm.

* solvent trace

3. Figures

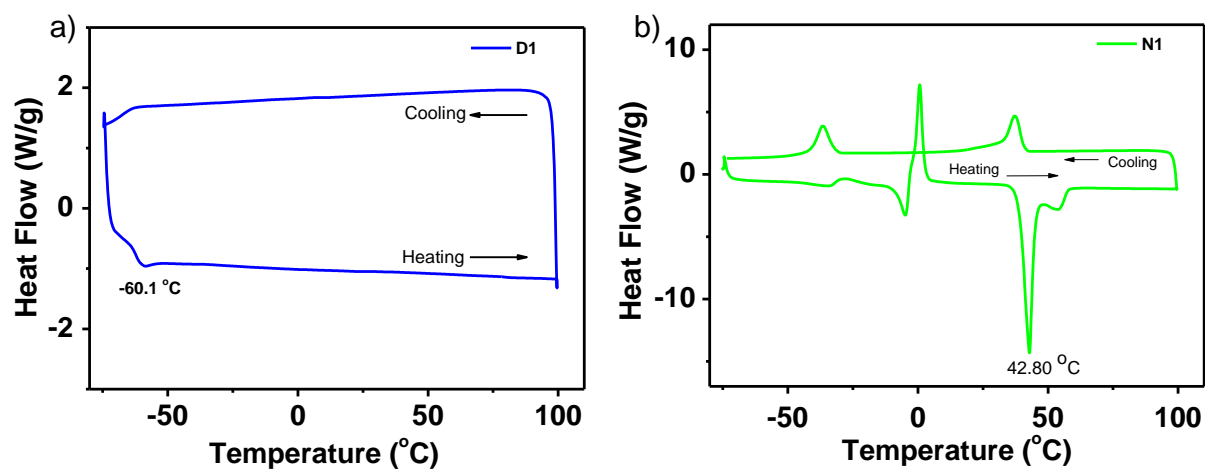


Figure S1. DSC thermograms in the heating trace at a scanning rate of 10 °C/min of a) **D1**, and b) **N1**.

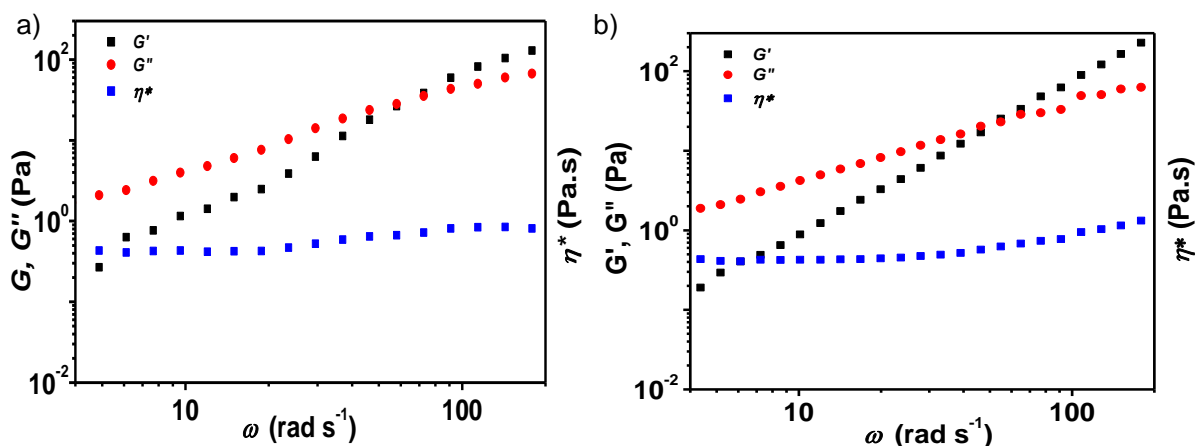


Figure S2. Variation of storage modulus (G') (■), loss modulus (G'') (●), and complex viscosity (η^*) (■) versus angular frequency on a double logarithmic scale, of a) **D1** and, b) **N1** ($\gamma = 0.1\%$).

The above figure is a double logarithmic curve of storage modulus (G') and loss modulus (G'') with angular frequency ranging from 0.1 to 200 rad s^{-1} of **N1** and **D1** under oscillatory shear ($\gamma = 0.1\%$). As the angular frequency varied from 0.1 to 200 rad s^{-1} , the storage modulus changed from 0.25 to 121 Pa, 0.20 to 221 Pa and the loss modulus changed from 2.1 to 69 Pa and 1.97 to 60 Pa, for **D1** and **N1**, respectively. It was evident that in the low-frequency region (0.1-20 rad s^{-1}), the loss modulus of the sample is $G'' > G'$ and in the high frequency region (21-200 rad s^{-1}), the trend is reversed $G' > G''$. Hence, it can be assumed that both **D1** and **N1** exhibit a viscous to elastic transition from low to high angular frequency. An increase of frequency gradually transforms the fluid to a semi-solid material indicating the characteristics of shear-hardening. A modulus intersection point G_i was appeared in the intermediate frequency region $\sim 20 \text{ rad s}^{-1}$, and at that point G' is found to be equal to G'' . It has to be noticed that before the G_i point, the loss modulus was always greater than the storage modulus and it indicates that upon deforming, the energy dissipation capacity of **D1** and **N1** is greater than the ability to store the elastic deformation energy. In short, the material shows viscous nature. However, after the G_i point, the storage modulus G' is greater than the loss modulus G'' , and both **D1** and **N1** exhibited elasticity with shear-hardening effect. Even though the storage modulus increased with angular frequency during this period, the growth rate was lower than before the G_i point. Interestingly, the loss modulus of both **D1** and **N1** showed an indication to decrease with the increase of angular frequency.

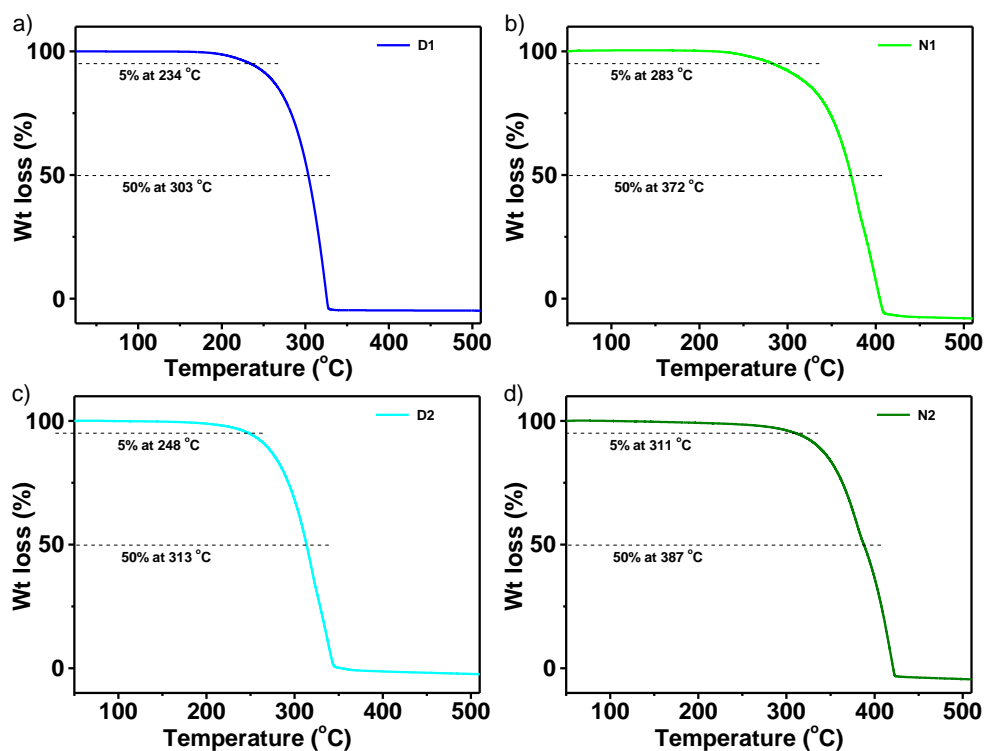


Figure S3. TGA of a) **D1**, b) **N1**, c) **D2**, and d) **N2**.

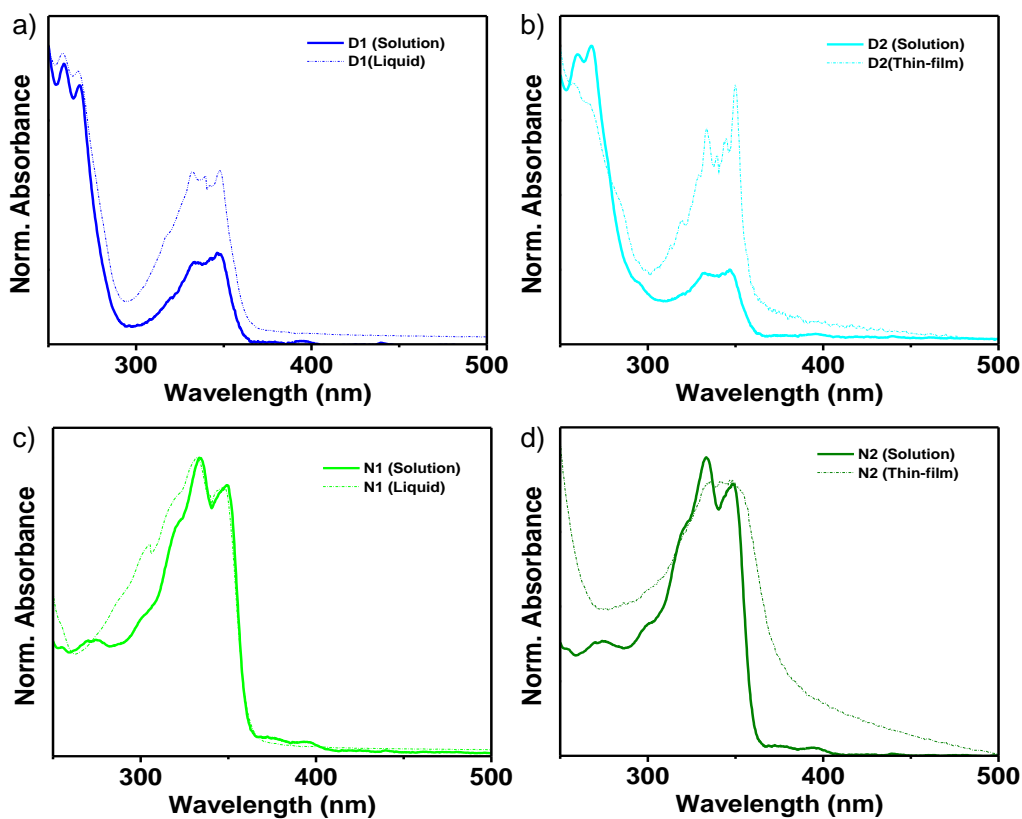


Figure S4. Normalized absorption of a) **D1**, b) **D2**, c) **N1** and, d) **N2** in dichloromethane (solid line) and liquid or thin film (dotted line).

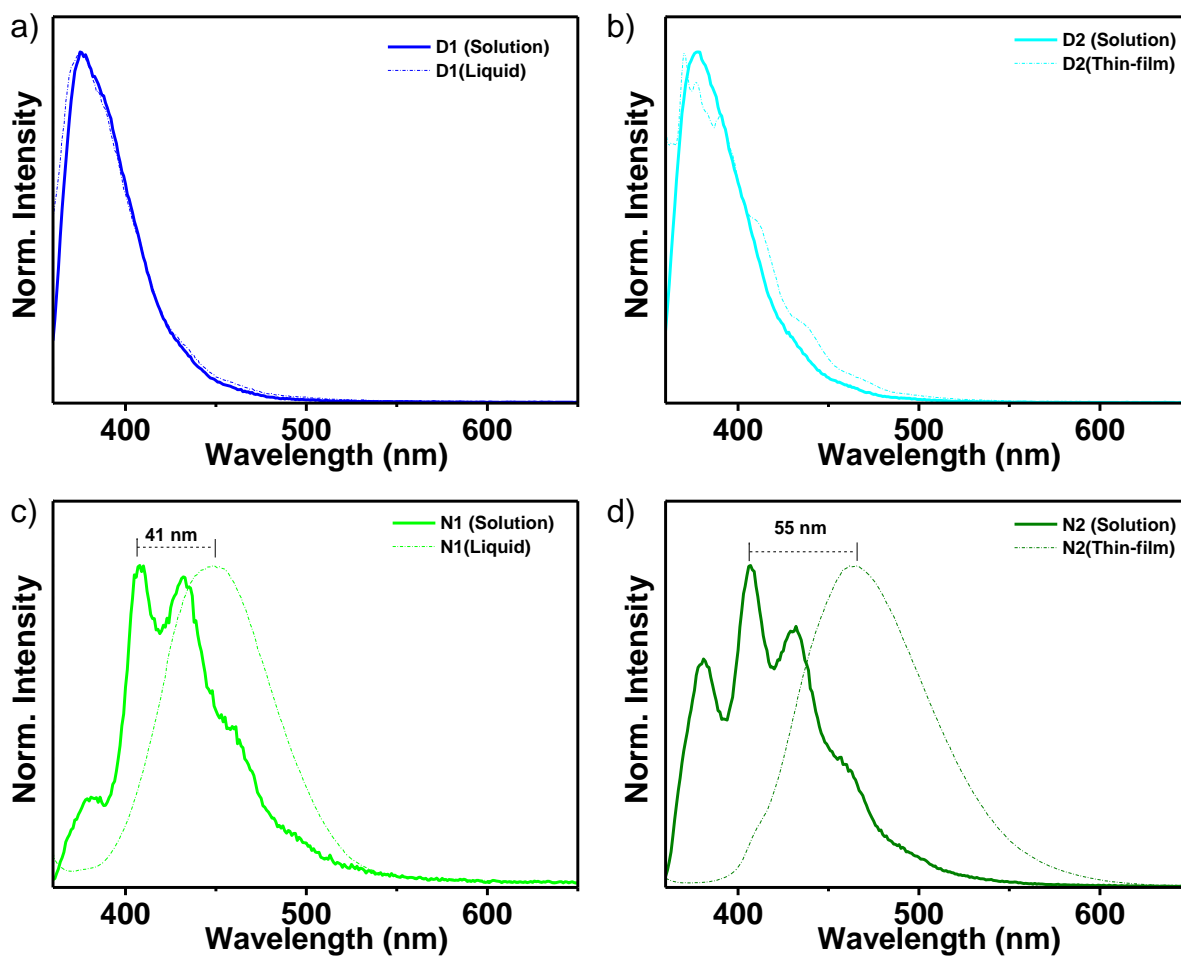


Figure S5. Normalized emission of a) **D1**, b) **D2**, c) **N1** and, d) **N2** in dichloromethane (solid line) and liquid or thin film (dotted line).

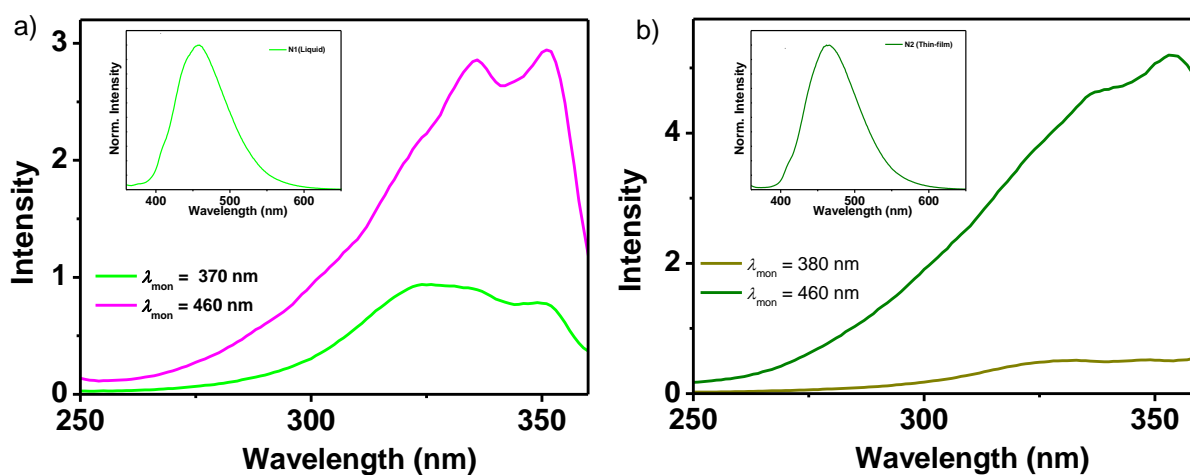


Figure S6. a) Excitation spectrum monitored at major emission peak of a) **N1** in the liquid state and b) **N2** in thin-film, insets show the corresponding emission spectra of liquid state and thin-film.

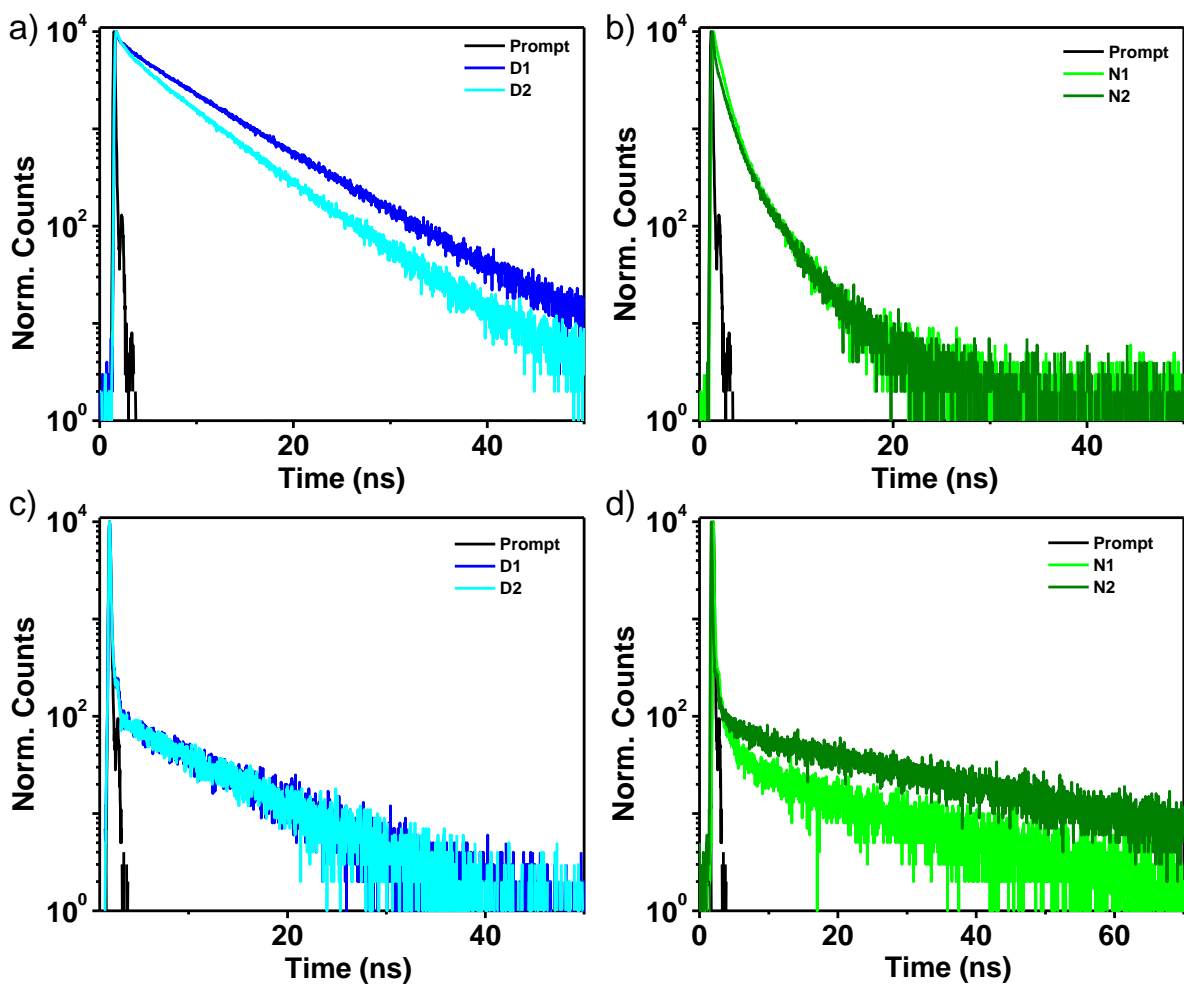


Figure S7. Emission lifetime decay profile of a) **D1**, and **D2** ($\lambda_{\text{mon}} = 390$ nm), b) **N1**, and **N2** ($\lambda_{\text{mon}} = 410$ nm) in dichloromethane, c) **D1**, and **D2** in thin flim ($\lambda_{\text{mon}} = 390$ nm), d) **N1**, and **N2** in neat state ($\lambda_{\text{mon}} = 460$ nm) at 25°C ($\lambda_{\text{ex}} = 374$ nm, $C = 1$ mM, $l = 1$ mm).

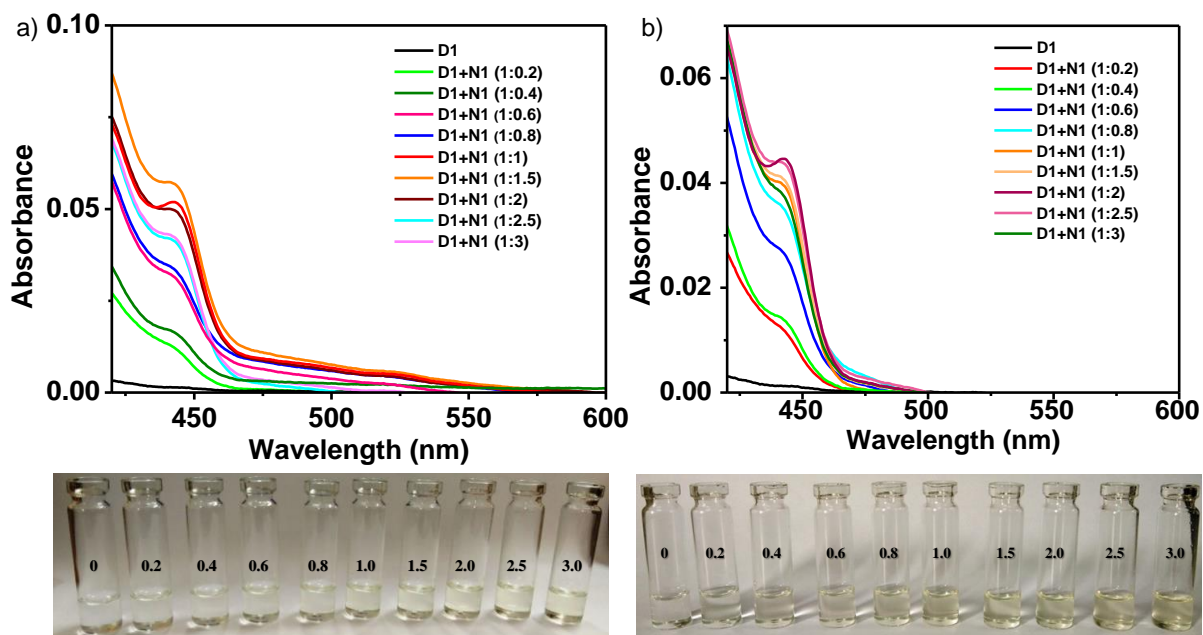


Figure S8. Variation in absorption spectra of **D1** with the increasing equivalence of **N1** in a) dichloromethane and b) *n*-hexane at 25 °C with corresponding solution photographs (bottom) ($C = 25 \text{ mM}$, $l = 1 \text{ cm}$).

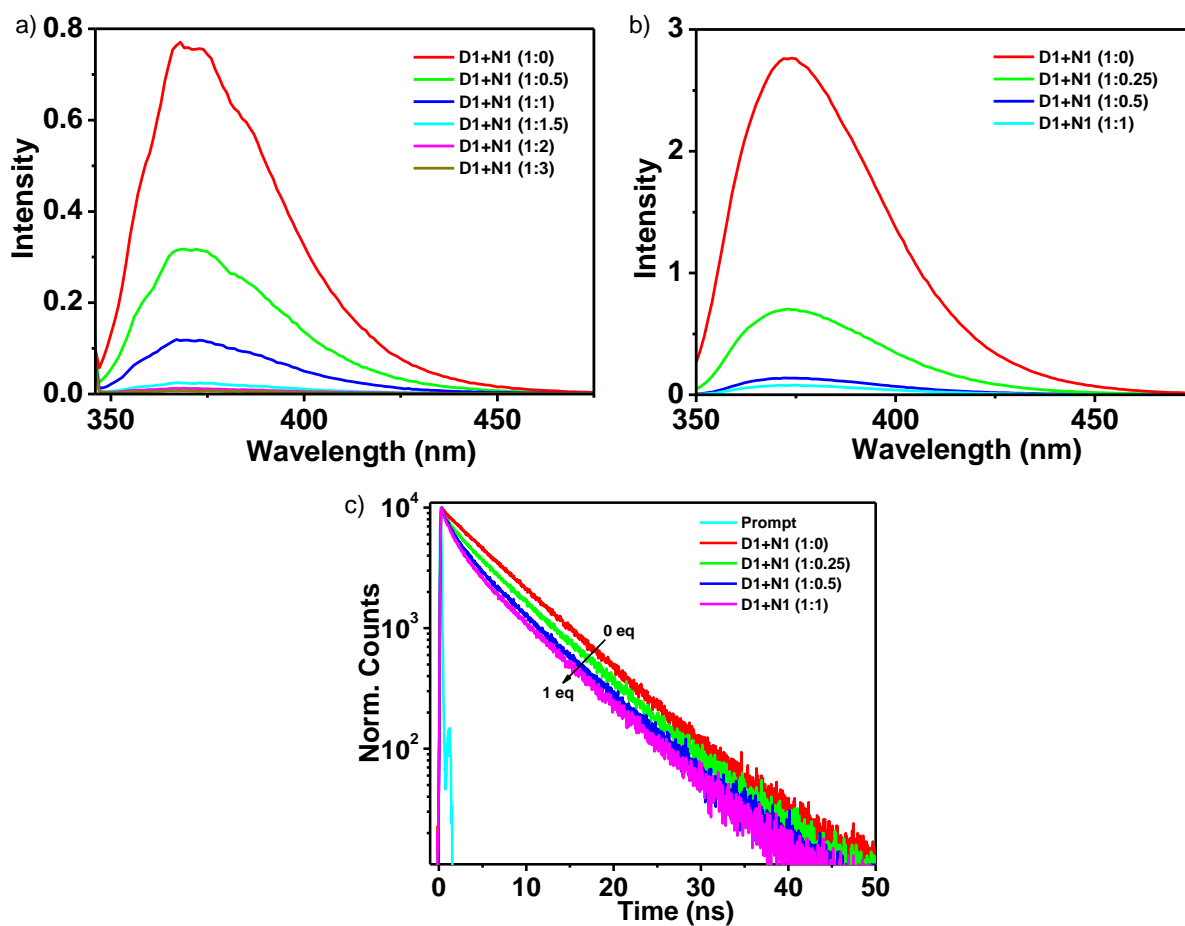


Figure S9. Variation in emission spectra of **D1** with an increasing equivalence of **N1** in a) *n*-hexane and b) acetonitrile at 25 °C and c) corresponding emission lifetime decay monitored at $\lambda_{\text{mon}} = 390$ nm and $\lambda_{\text{ex}} = 374$ nm in acetonitrile at 25 °C. ($C = 25$ mM, $l = 1$ cm, $\lambda_{\text{ex}} = 350$ nm).

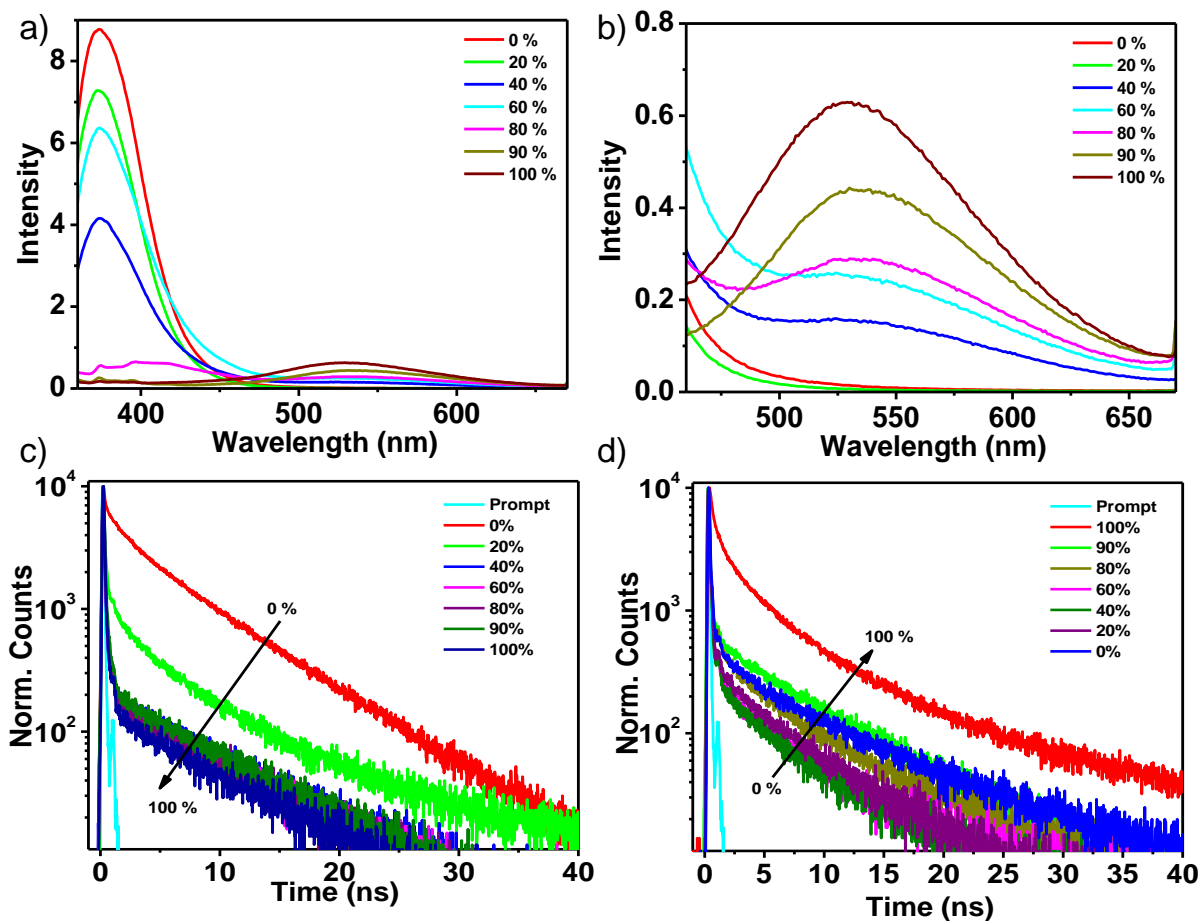


Figure S10. a) Variation in emission spectra of **D1:N1** (1:1) ($C = 1 \times 10^{-4}$ M) with increasing % of water b) and zoom spectra from 400 to 700 nm and the corresponding emission lifetime decay monitored at c) $\lambda_{\text{mon}} = 390$ nm, and d) $\lambda_{\text{mon}} = 530$ nm, ($\lambda_{\text{ex}} = 374$ nm).

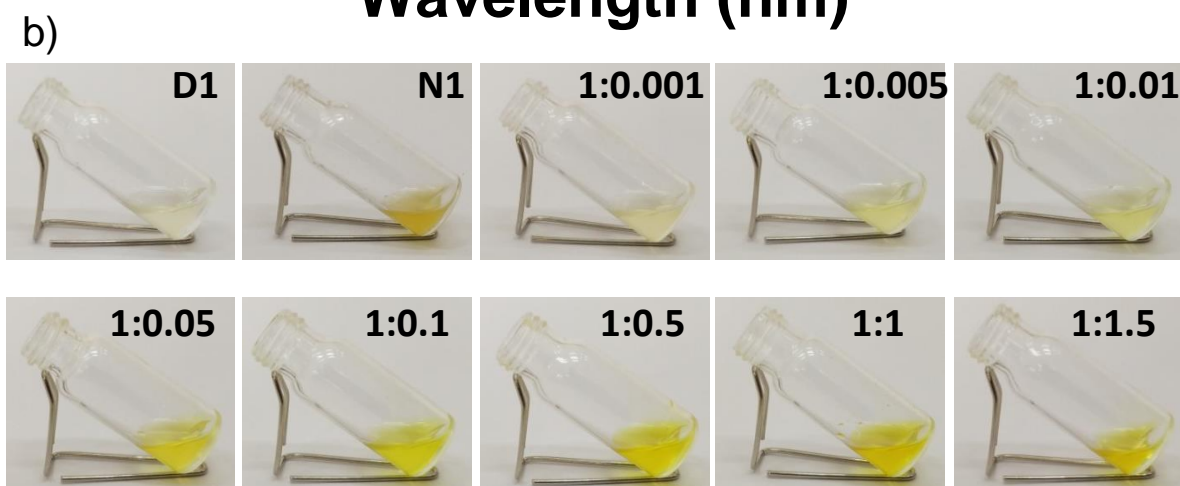
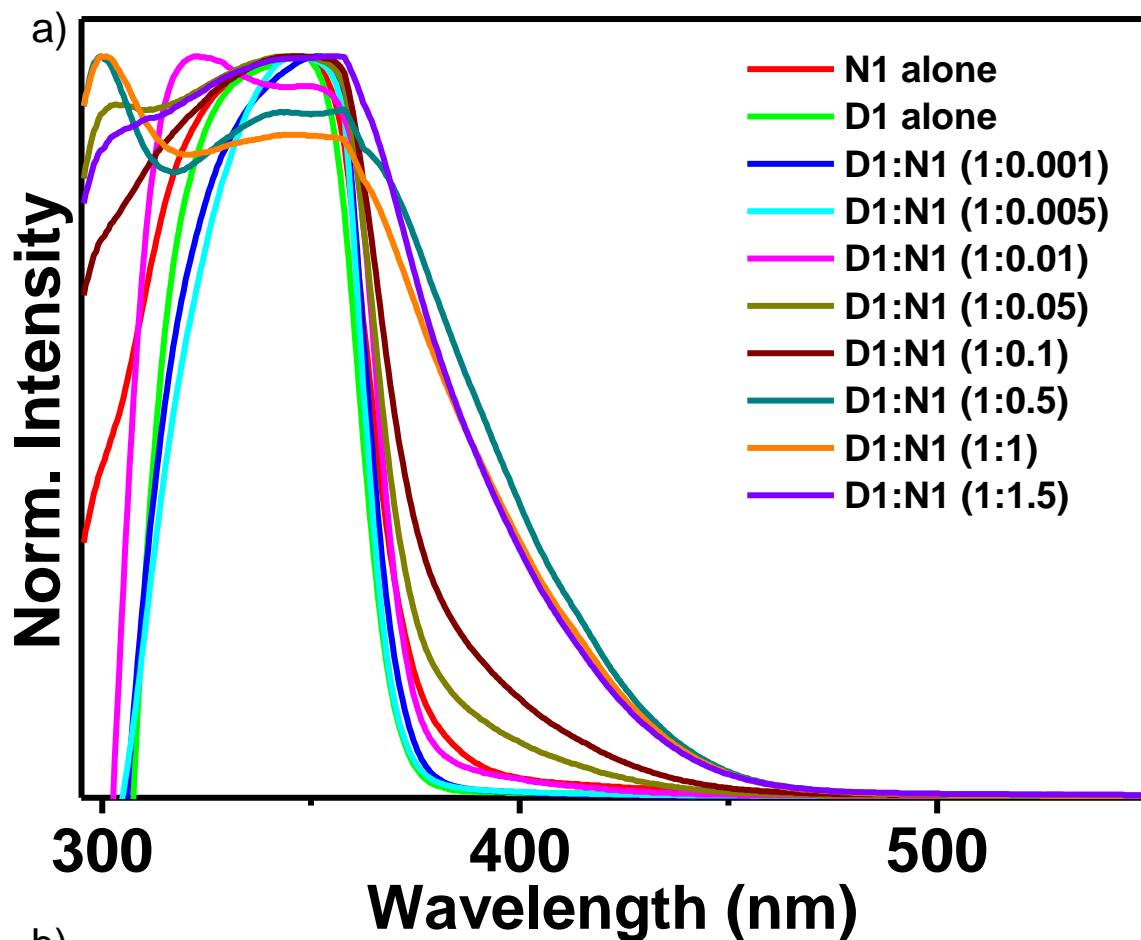


Figure S11. a) Absorption spectral changes of **D1** with an increasing equivalence of **N1** and b) corresponding day-light photographs.

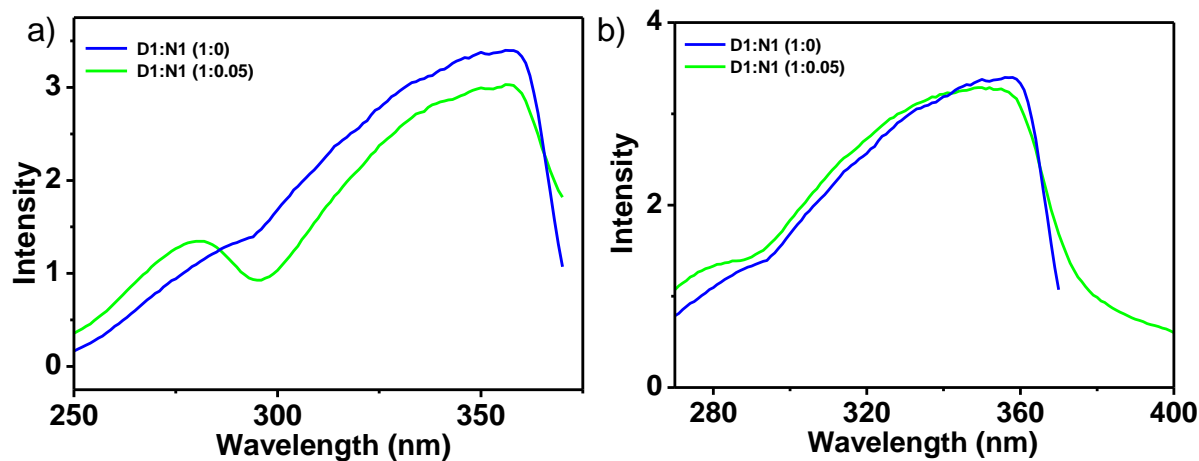


Figure S12. a) Excitation spectrum of **EL** monitored at a) $\lambda_{\text{mon}} = 380$ nm and b) $\lambda_{\text{mon}} = 530$ nm ($\lambda_{\text{ex}} = 250\text{-}420$ nm).

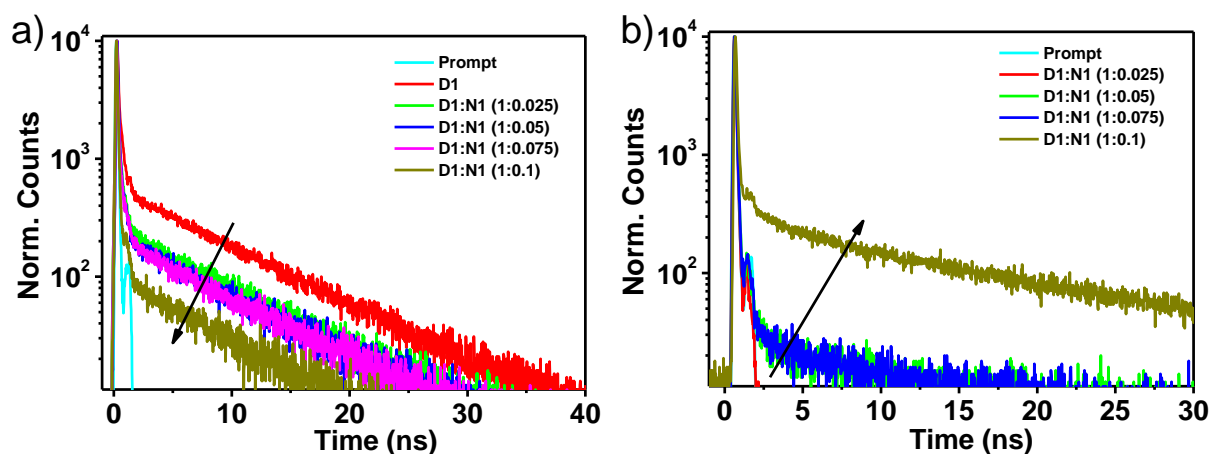


Figure S13. Emission lifetime decay profiles of **EL**, a) $\lambda_{\text{mon}} = 390$ nm, and b) $\lambda_{\text{mon}} = 530$ nm ($\lambda_{\text{ex}} = 374$ nm).

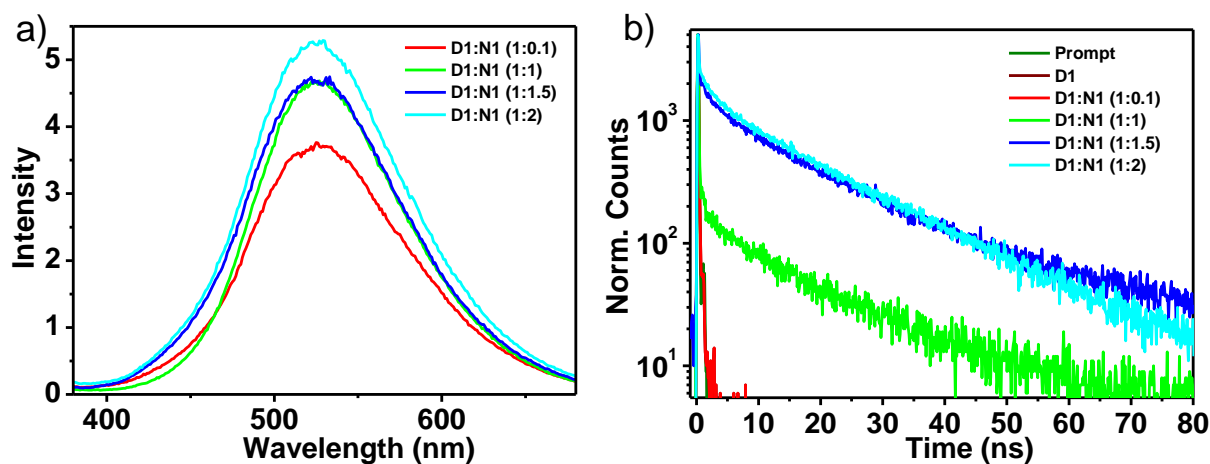


Figure S14. a) Variation in emission spectra of **D1** with an increasing equivalence of **N1** and b) corresponding emission lifetime decay monitored at $\lambda_{\text{mon}} = 540$ nm ($\lambda_{\text{ex}} = 374$ nm).

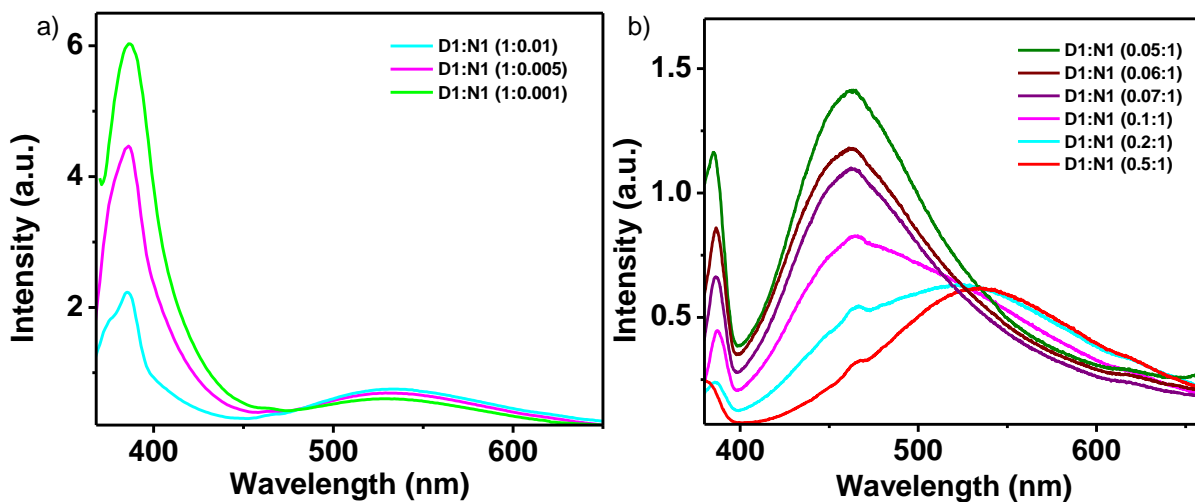


Figure S15. a) Variation of steady-state emission of **EL** with a lower equivalence of **N1**, b) Variation of steady-state emission of **N1** with an increasing equivalence of **D1** in the solvent-free liquid ($\lambda_{\text{ex}} = 350$ nm).

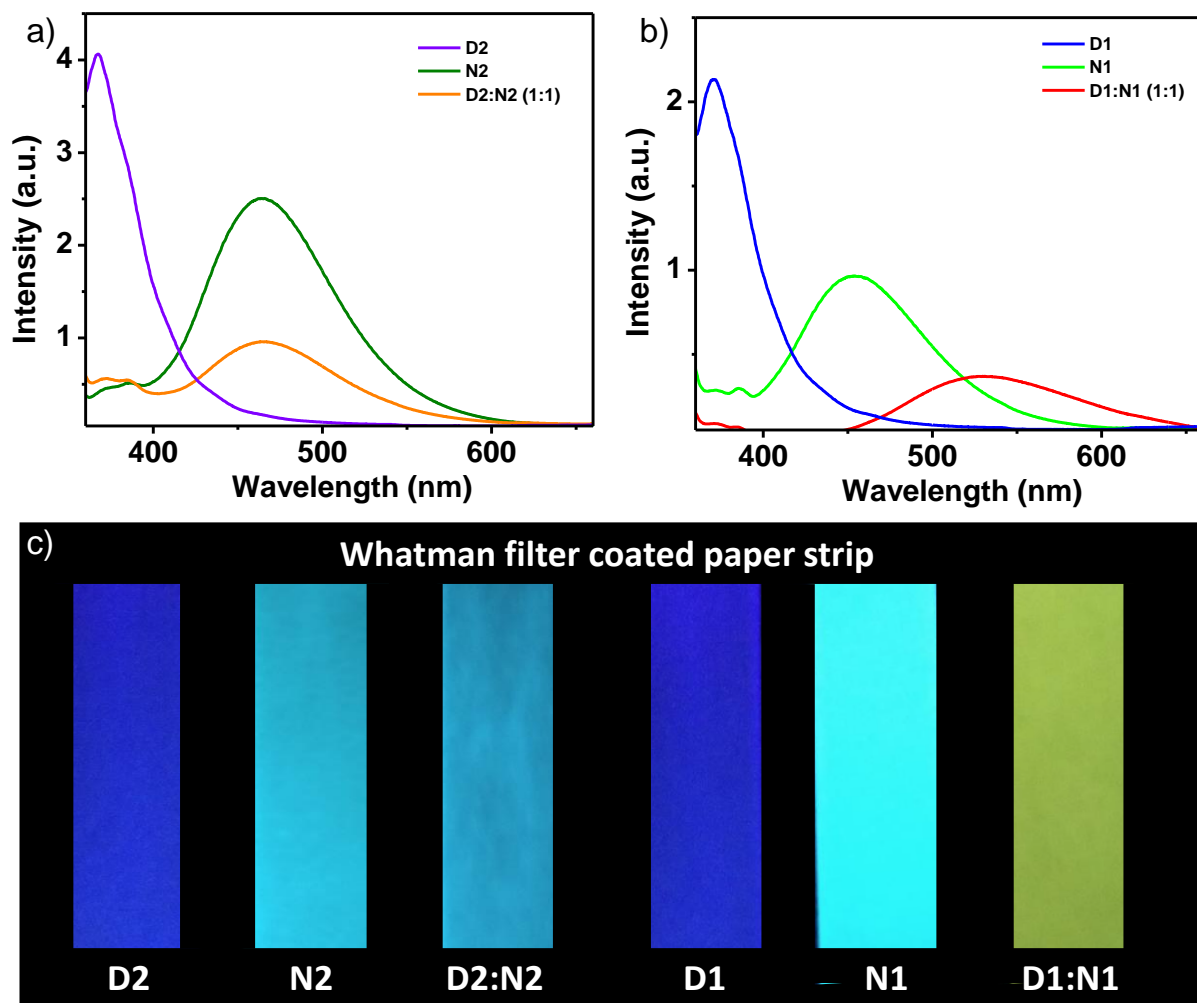


Figure S16. a) Steady-state emission spectra of a) **D2**, **N2**, and **D2:N2** (1:1), b) **D1**, **N1**, and **D1:N1** (1:1) coated on Whatman Filter paper from dichloromethane solution (1 mM) and c) corresponding photographs after excitation in the dark ($\lambda_{\text{ex}} = 365 \text{ nm}$).

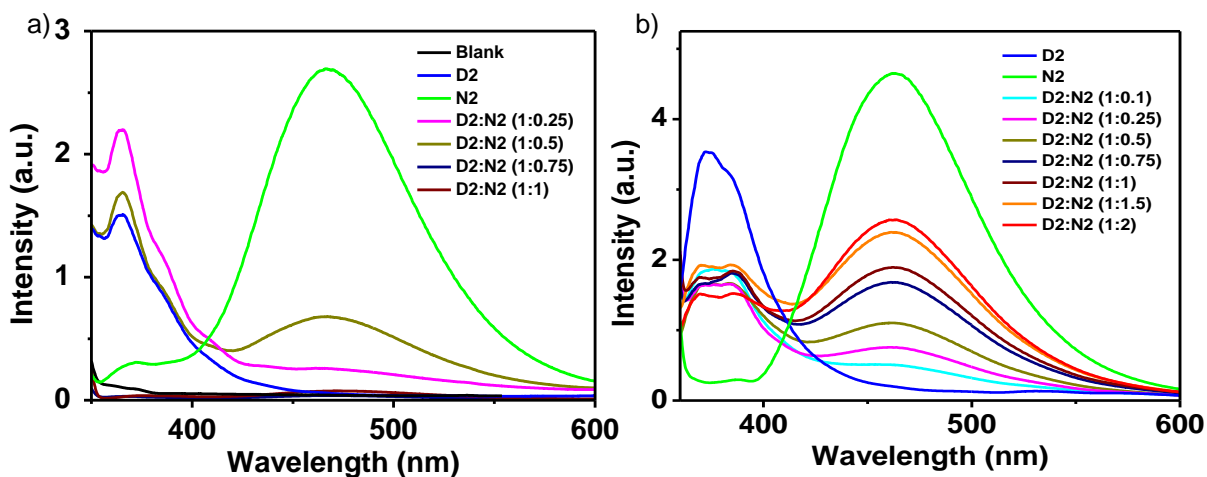


Figure S17. Variation in emission spectra of **D2** with an increasing equivalence of **N2** a) coated on Whatman Filter paper and b) in solid-state ($\lambda_{\text{ex}} = 350 \text{ nm}$).

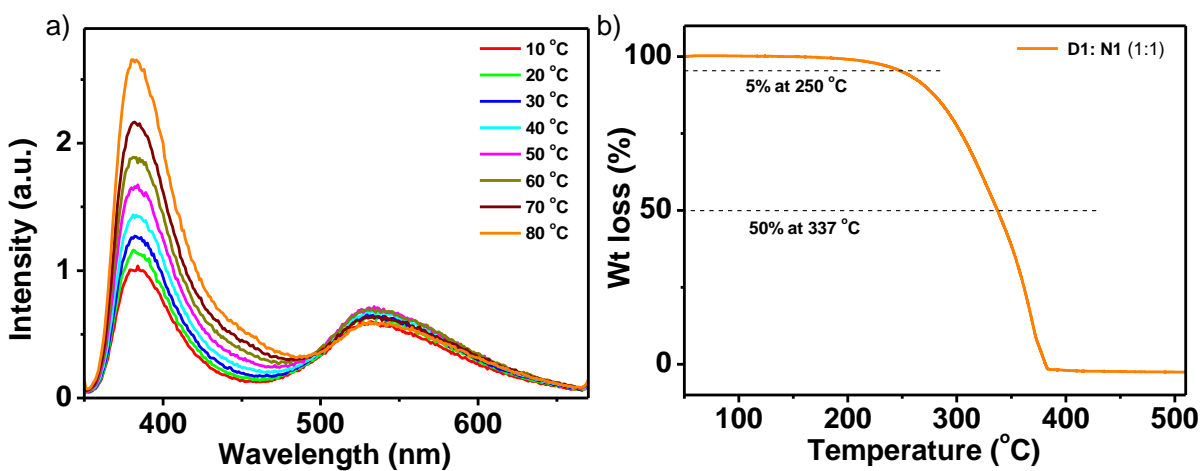


Figure S18. a) Variable temperature steady-state emission spectra of **D1:N1** and b) TGA of **D1:N1** (1:1).

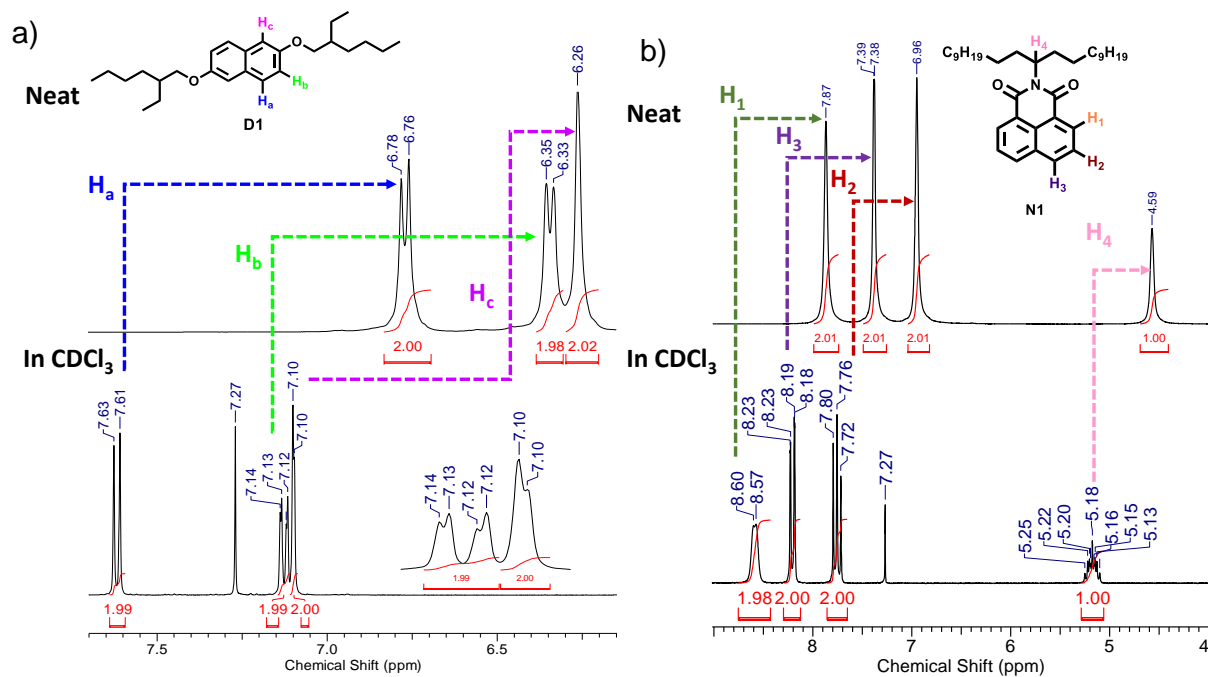


Figure S19. Comparison of ^1H NMR spectra of a) **D1** and b) **N1** in solvent-free liquid and CDCl_3 solution.

A comparison of the ^1H NMR spectra of the molecules in CDCl_3 and the neat state (external reference DMSO-d_6) show that all signals shift upfield and become broad.

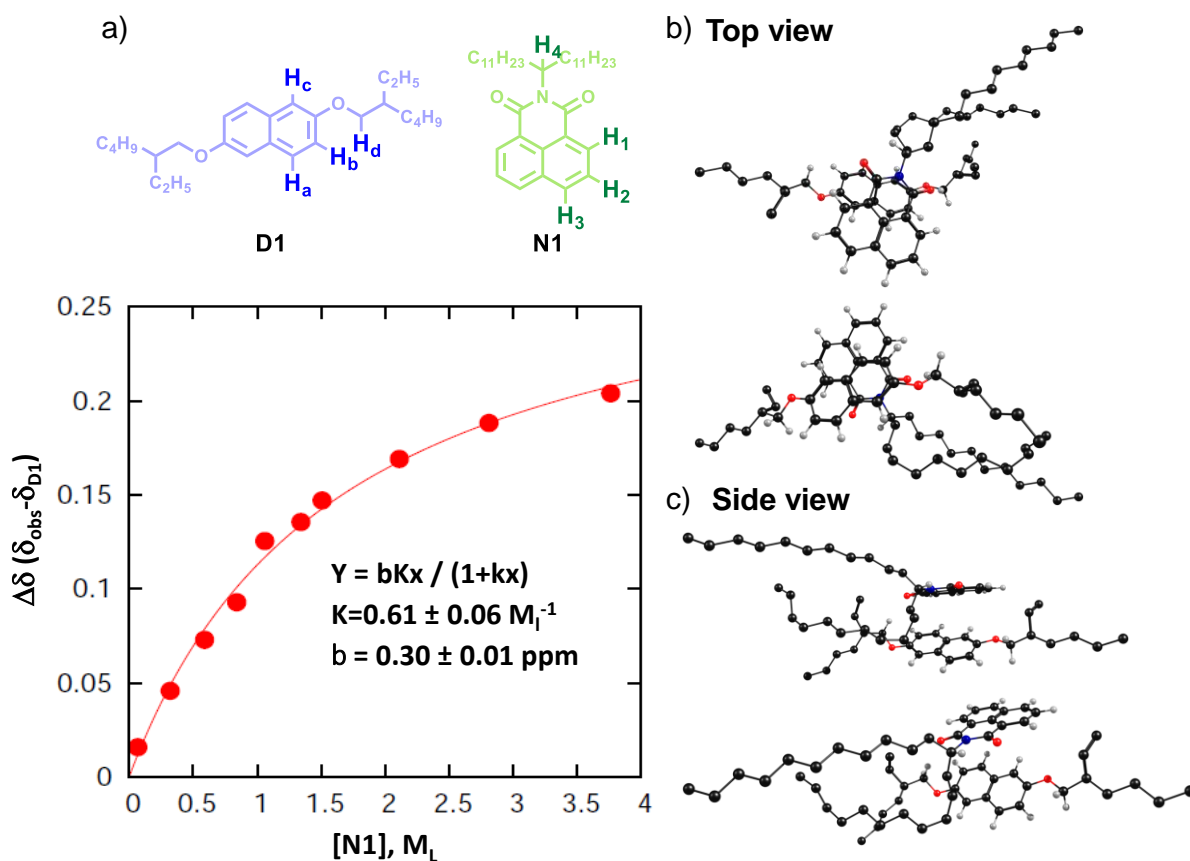


Figure S20. a) The relative shift of H_d with respect to the position in neat **D1** as a function of **N1** concentration at 318 K. b) Top and c) side view of the stacked dimer of **D1:N1**.

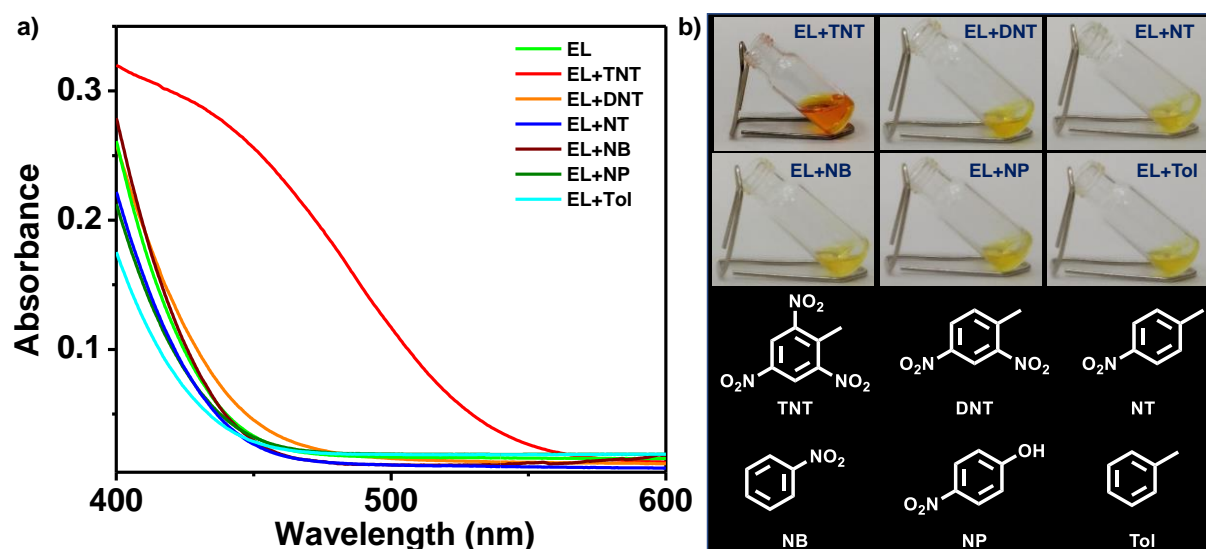


Figure S21. a) Absorption spectral changes of **EL** in contact with different acceptors, b) corresponding day-light photographs, and chemical structures of used acceptors (acceptor loading is 1 wt %).

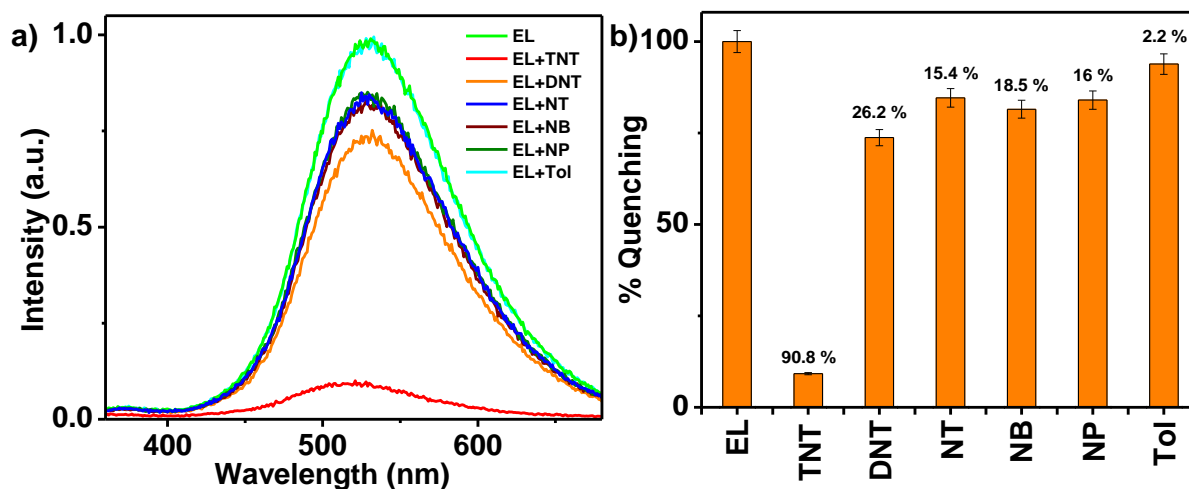


Figure S22. a) Steady-state emission spectral changes, and b) corresponding emission quenching % of **EL** with different acceptors ($\lambda_{\text{ex}} = 350$ nm, acceptor loading is 1 wt %, 3% error bar).

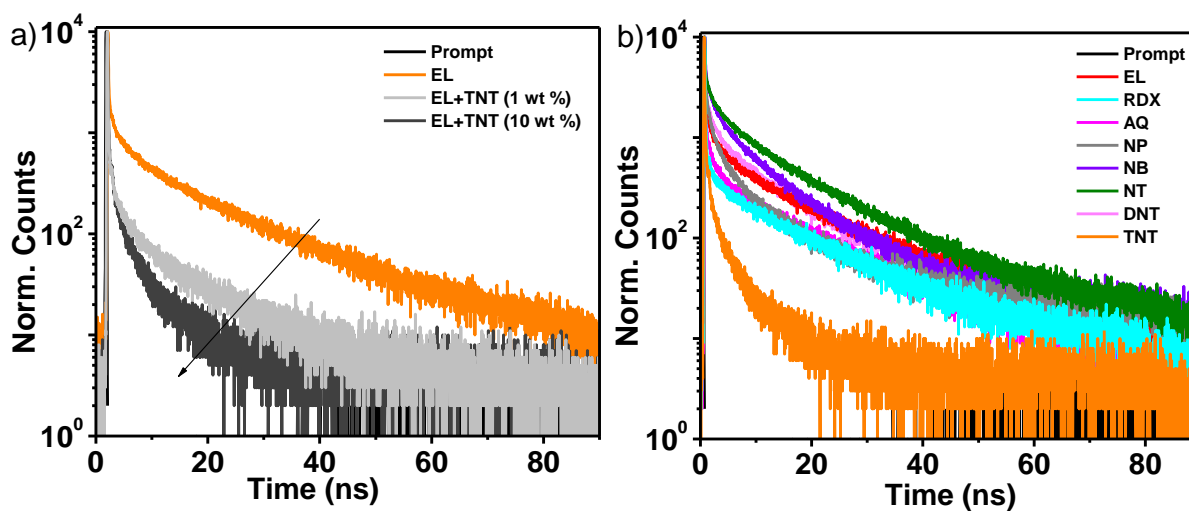


Figure S23. Lifetime decay profile with acceptors a) **EL**, **EL+1 wt % TNT** and **EL+10 wt % TNT**, and b) **EL** with different acceptor (10 weight %) monitor at $\lambda_{\text{mon}} = 530$ nm ($\lambda_{\text{ex}} = 374$ nm).

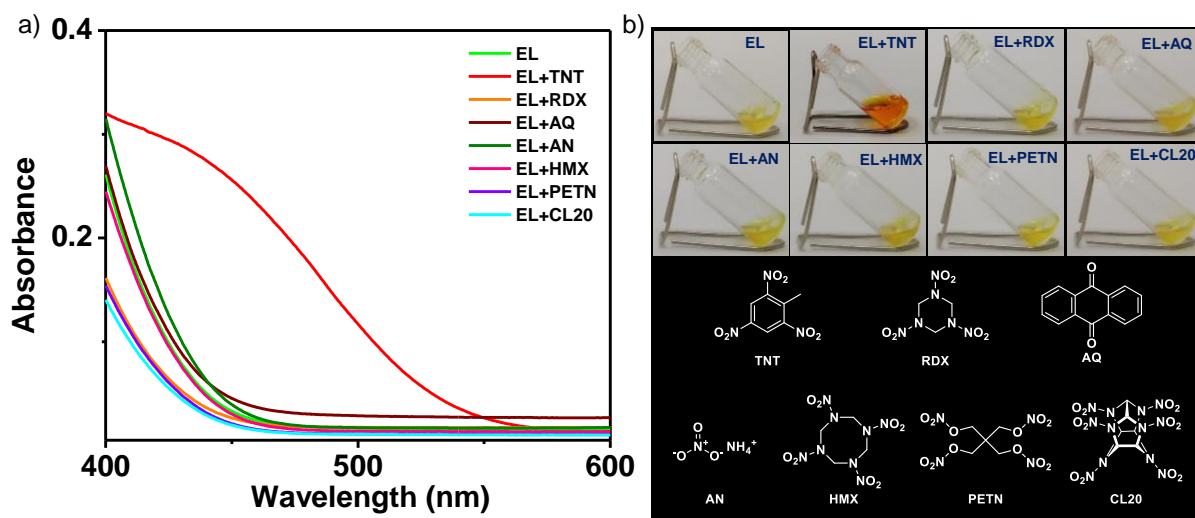


Figure S24. a) Absorption spectral changes of **EL** contact with different acceptors and, b) corresponding day-light photographs and chemical structures of used acceptors (acceptor loading is 1 wt %).

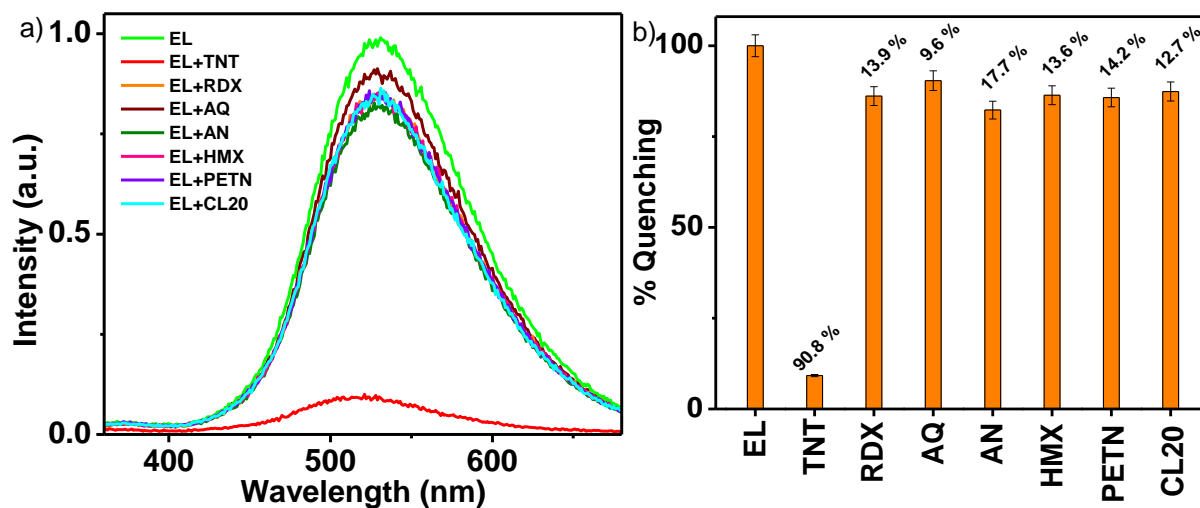


Figure S25. a) Steady-state emission spectral changes and b) variation of emission quenching % of **EL** with different acceptors ($\lambda_{\text{ex}} = 350$ nm, acceptor loading is 1 wt %, 3% error bar).

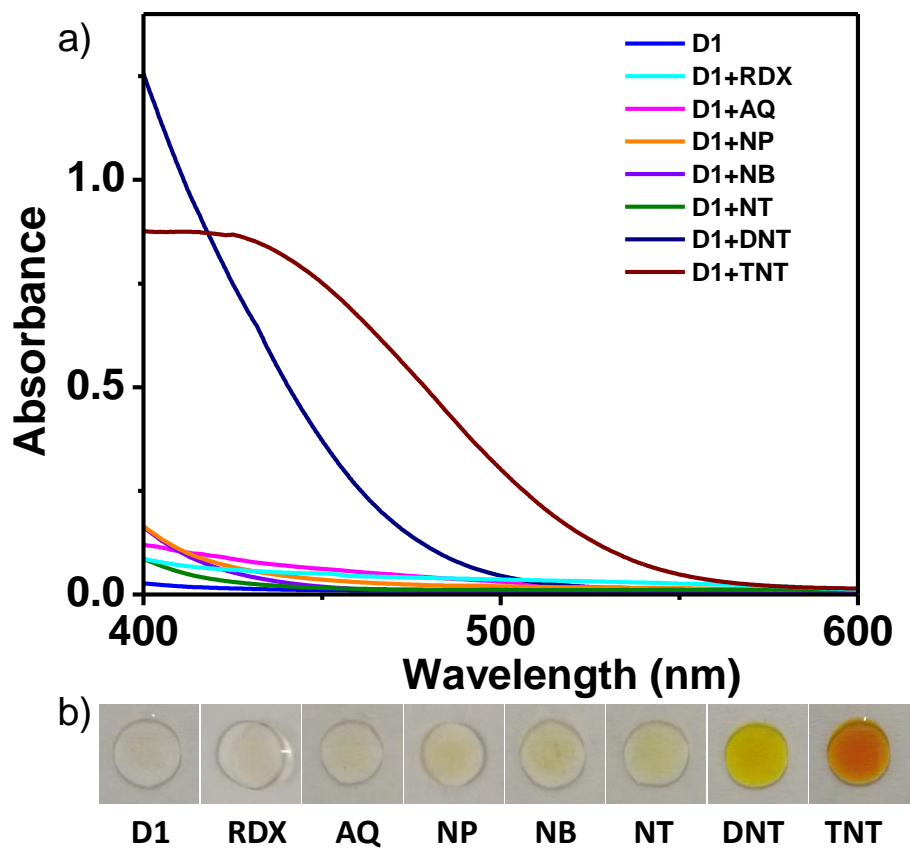


Figure S26. a) Absorption spectral changes of **D1** contact with different acceptors and b) corresponding day-light photographs (acceptor loading is 1 wt %).

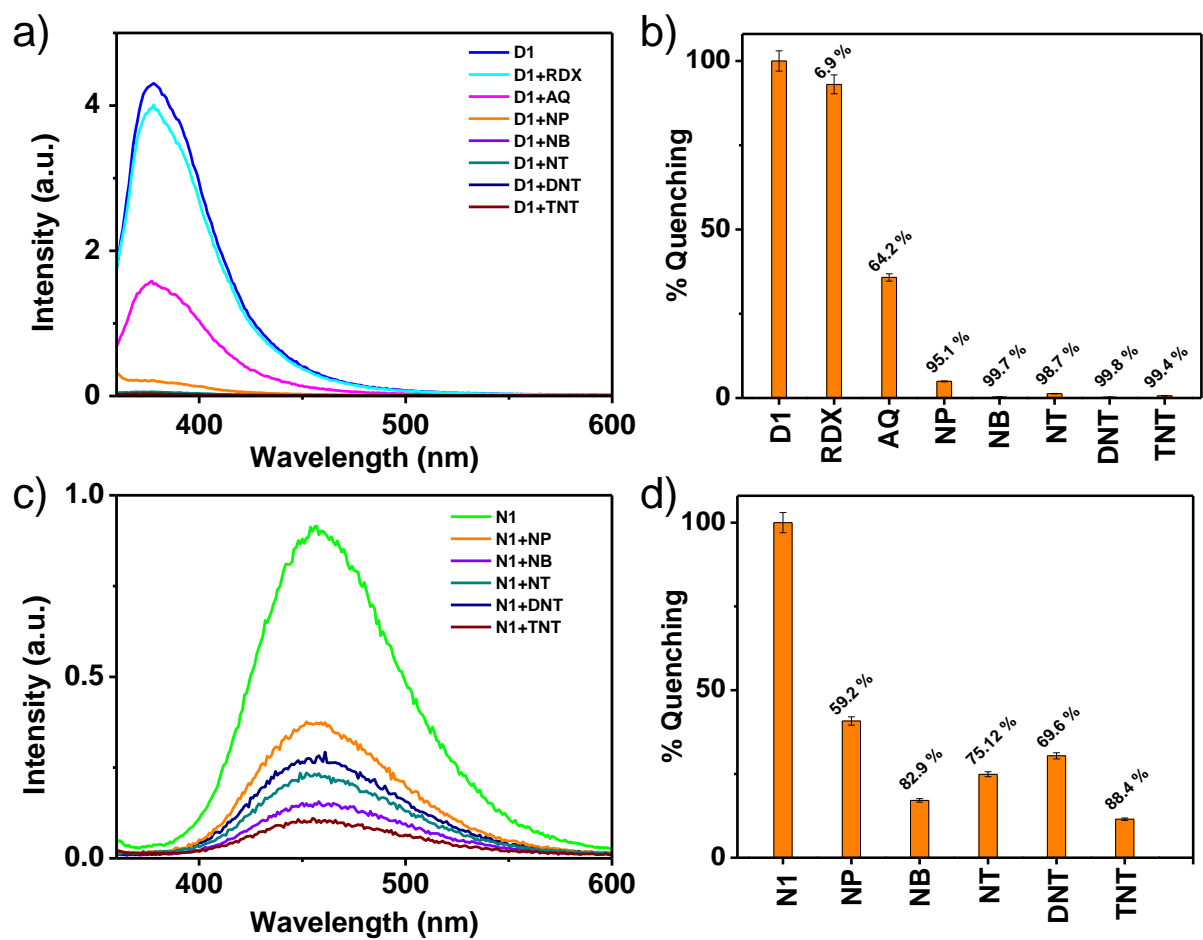


Figure S27. a), c) Steady-state emission spectral changes and b), d) variation of emission quenching % of **D1** and **N1** different acceptors, respectively ($\lambda_{\text{ex}} = 350$ nm, acceptor loading is 1 wt %, 3% error bar).

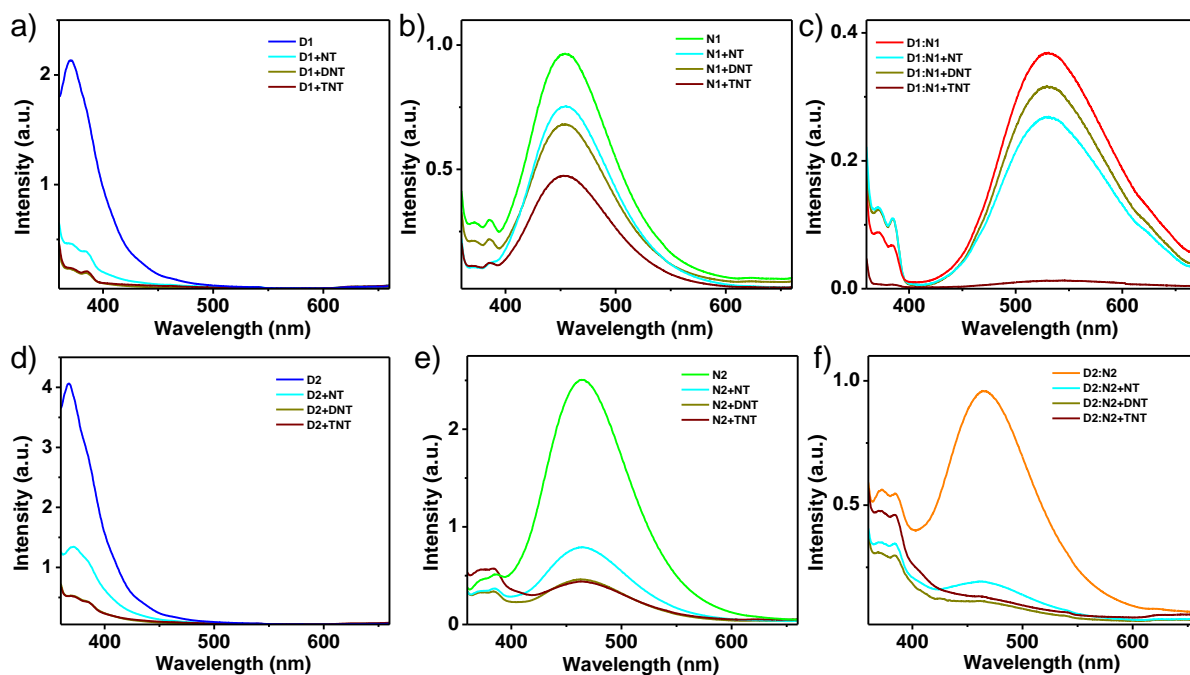


Figure S28. a) Variation in emission spectra of a) **D1**, b) **N1**, c) **D1:N1** (1:1), d) **D2**, e) **N2**, and f) **D2:N2** (1:1) with NT, DNT, and TNT, coated on Whatman Filter paper (concentration of compounds and acceptors 1 mM).

*In all the above experiments, except **EL**, no selectivity is observed. It points to the importance of the solvent-free liquid medium, which assists the donor, acceptor molecules to form stable exciplex, and thus enable dual-mode selective sensing of TNT. We attempted the same experiments using **EL** coated Whatman filter paper and large-area coating on quartz plates and found that both the test devices work as perfectly as the neat liquid and deliver the same selectivity.*

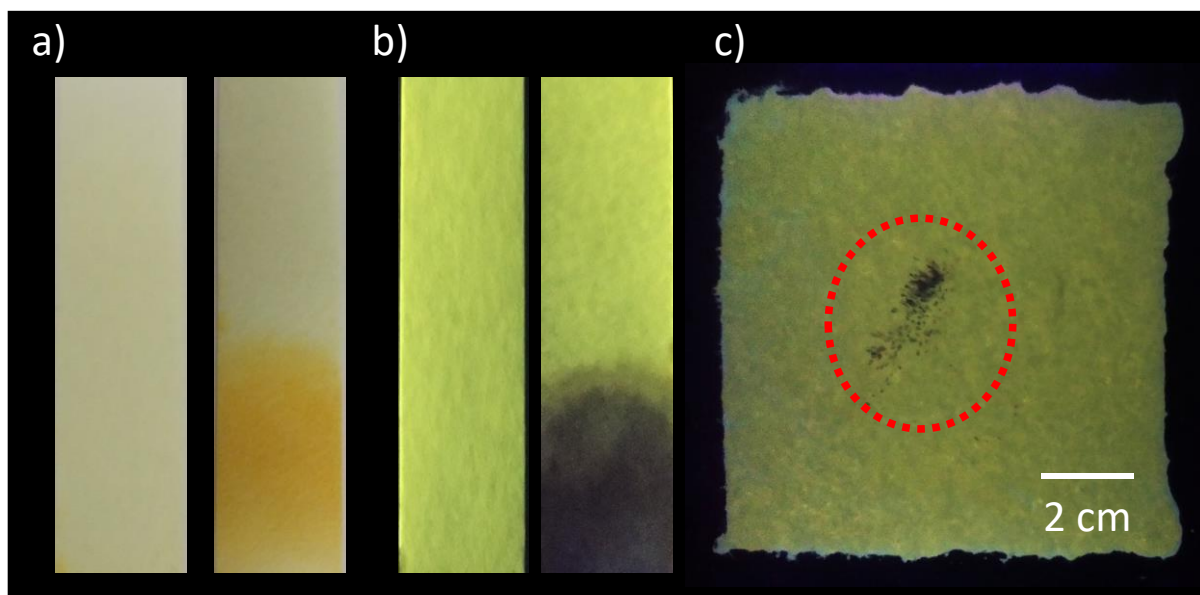


Figure S29. Photographs of **EL** coated paper strips showing a) visible color change and b) emission quenching with TNT under UV light (365 nm). c) The emission quenching of **EL** coated on a large area with TNT under UV light (365 nm).

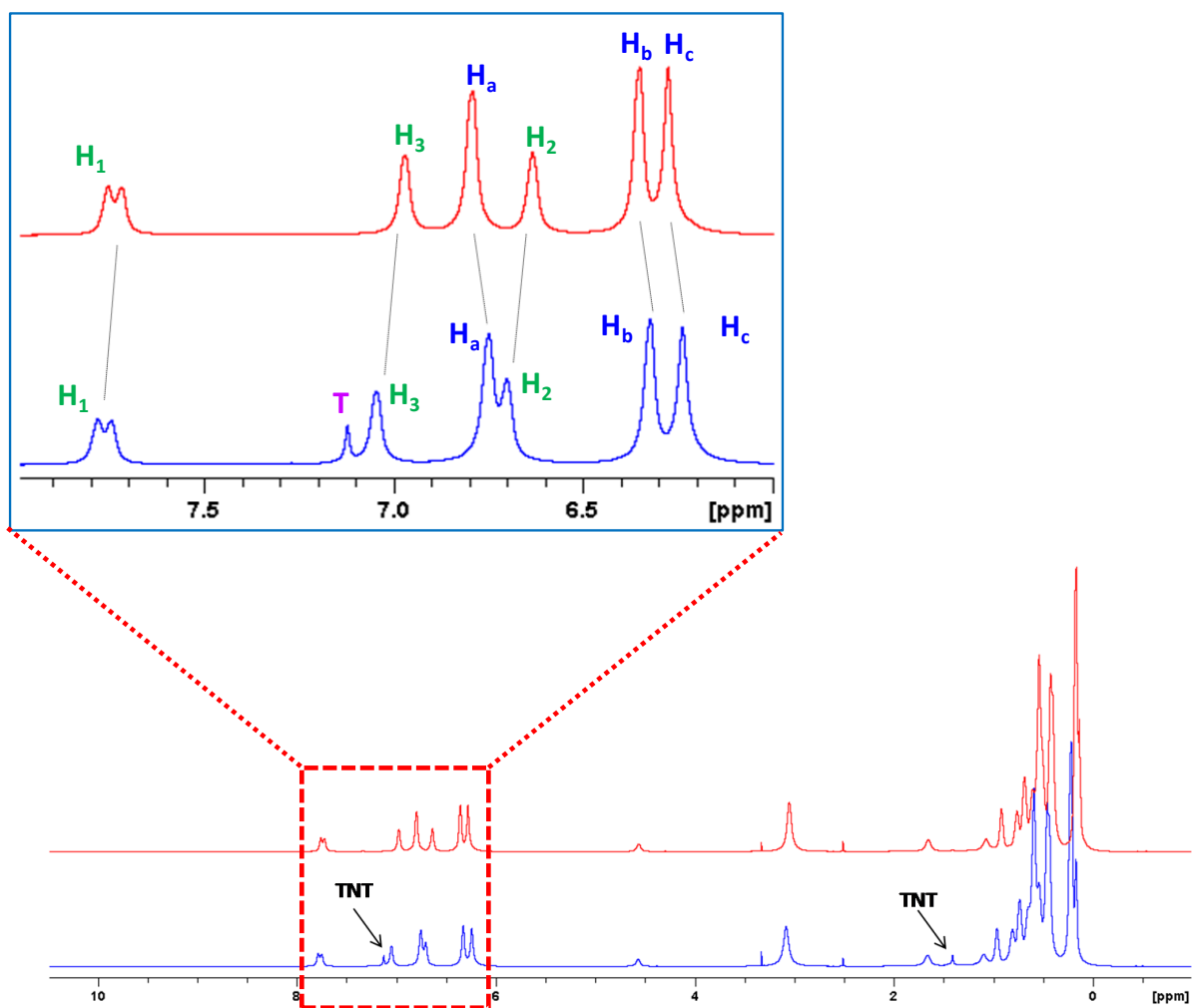


Figure S30. ¹H NMR spectrum of EL (D1:N1=1:0.5) at 298 K with (blue) and without (red) TNT (5 wt%).

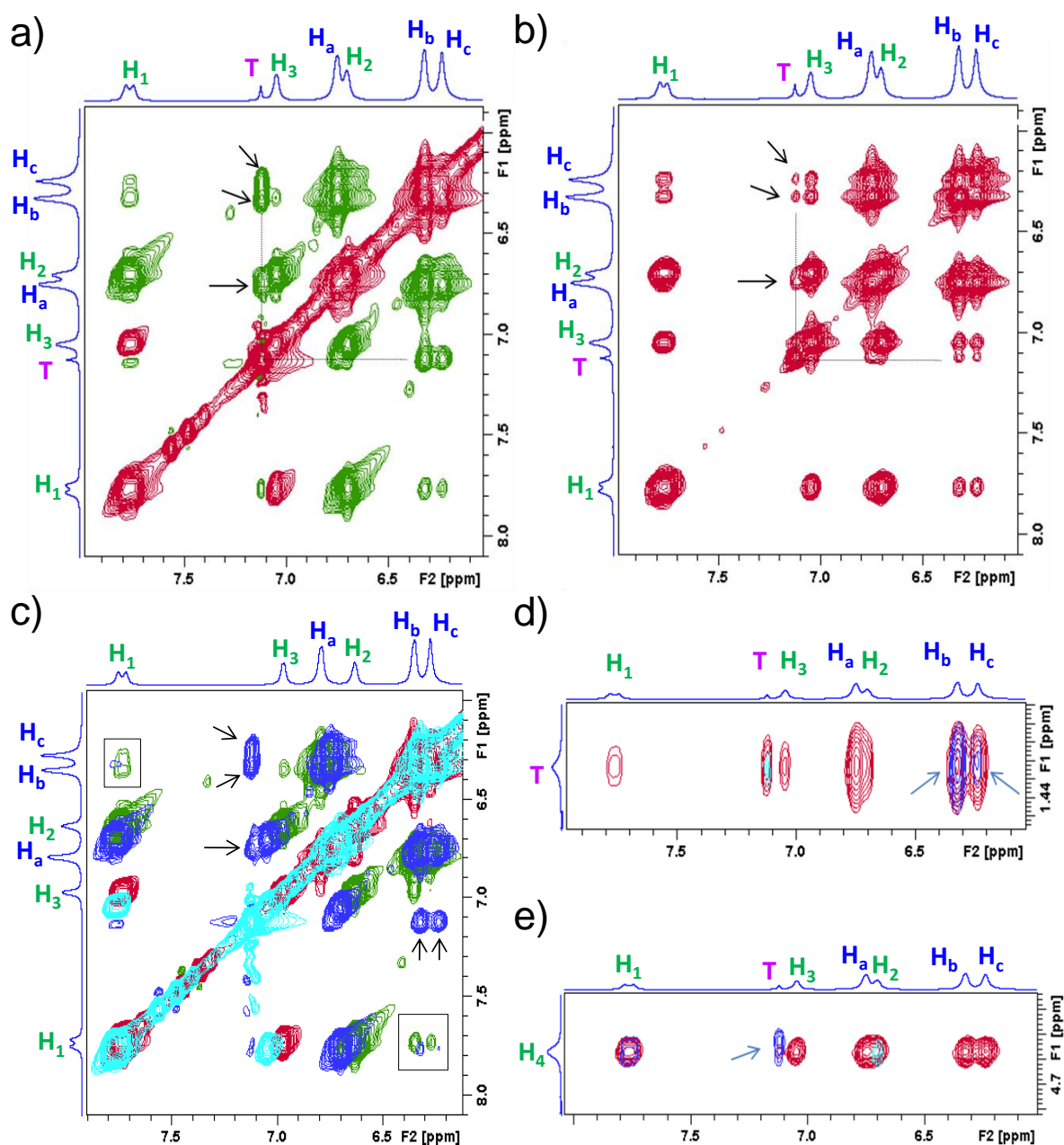


Figure S31. 2D NMR spectra of **EL** (**D1:N1**=1:0.5) in presence of TNT at 298 K. Aromatic regions of a) ROESY and b) NOESY spectra with intermolecular crosspeaks between **EL** and TNT indicated by arrows. c) Overlay of ROESY spectra with (green/red) and without (blue/purple) TNT. Weakened **D1-N1** cross peaks in presence of TNT are shown in boxes whereas the strong **D1-TNT** cross peaks are indicated by arrows. Overlay of slices from ROESY (purple) and NOESY (red) showing cross peaks of d) methyl protons of TNT and e) H₄ proton of **N1** (ROESY crosspeaks between TNT and **EL** are indicated by arrows).

Tables

Table S1. Emission lifetime of **D1**, **D2**, **N1** and **N2** in dichloromethane ($C = 1 \text{ mM}$, $l = 1 \text{ mm}$, $\lambda_{\text{ex}} = 374 \text{ nm}$).

| Sr. No | Compounds | Wavelength monitored (nm) | Lifetime |
|--------|-----------|---------------------------|---|
| 1 | D1 | 390 | $\tau_1 = 0.42 \text{ ns (3.63 \%)}$ $\tau_2 = 7.02 \text{ ns (96.37 \%)}$ |
| 2 | D2 | 390 | $\tau_1 = 0.7 \text{ ns (8.75 \%)}$ $\tau_2 = 5.78 \text{ ns (91.25 \%)}$ |
| 3 | N1 | 410 | $\tau_1 = 0.8 \text{ ns (71.07 \%)}$ $\tau_2 = 2.88 \text{ ns (28.93 \%)}$ |
| 4 | N2 | 410 | $\tau_1 = 0.84 \text{ ns (64.5 \%)}$ $\tau_2 = 2.99 \text{ ns (35.5 \%)}$ |

Table S2. Emission lifetime of **D1**, **D2**, **N1**, and **N2** in thin-film ($\lambda_{\text{ex}} = 374 \text{ nm}$).

| Sr. No | Compounds | Wavelength monitored (nm) | Lifetime |
|--------|-----------|---------------------------|--|
| 1 | D1 | 390 | $\tau_1 = 0.09 \text{ ns (71.21 \%)}$ $\tau_2 = 7.59 \text{ ns (28.29 \%)}$ |
| 2 | D2 | 390 | $\tau_1 = 0.09 \text{ ns (79.89 \%)}$ $\tau_2 = 7.44 \text{ ns (20.11 \%)}$ |
| 3 | N1 | 460 | $\tau_1 = 0.018 \text{ ns (90.42 \%)}$ $\tau_2 = 17.56 \text{ ns (9.48 \%)}$ |
| 4 | N2 | 460 | $\tau_1 = 0.014 \text{ ns (78.23 \%)}$ $\tau_2 = 26.97 \text{ ns (21.77 \%)}$ |

Table S3. Emission lifetime of **D1:N1** in acetonitrile (0.1 mM) ($\lambda_{\text{mon}} = 390$ nm, $\lambda_{\text{ex}} = 374$ nm).

| Sr. No | Sample (D1:N1) | Lifetime |
|--------|----------------|--|
| 1 | 1:0 | $\tau_1 = 0.51$ ns (2.18 %) $\tau_2 = 6.66$ ns (97.82 %) |
| 2 | 1:0.25 | $\tau_1 = 0.96$ ns (6.86 %) $\tau_2 = 6.58$ ns (93.14 %) |
| 3 | 1:0.5 | $\tau_1 = 1.22$ ns (14.83 %) $\tau_2 = 6.52$ ns (85.17 %) |
| 4 | 1:1 | $\tau_1 = 1.18$ ns (17.7 %) $\tau_2 = 6.41$ ns (82.3 %) |

Table S4. Emission lifetime of **D1:N1** (1:1) in acetonitrile with increasing % of water ($C = 0.1$ mM, $\lambda_{\text{mon}} = 390$ nm, $\lambda_{\text{ex}} = 374$ nm).

| Sr. No | % of water | Lifetime |
|--------|------------|--|
| 1 | 0 | $\tau_1 = 0.80$ ns (12.91 %) $\tau_2 = 6.64$ ns (87.09 %) |
| 2 | 20 | $\tau_1 = 0.11$ ns (32.95 %) $\tau_2 = 6.32$ ns (67.05 %) |
| 3 | 40 | $\tau_1 = 0.04$ ns (62.44 %) $\tau_2 = 8.26$ ns (37.56 %) |
| 4 | 60 | $\tau_1 = 0.04$ ns (65.71 %) $\tau_2 = 7.92$ ns (34.29 %) |
| 5 | 80 | $\tau_1 = 0.05$ ns (65.56 %) $\tau_2 = 7.87$ ns (34.44 %) |
| 6 | 90 | $\tau_1 = 0.06$ ns (60.04 %) $\tau_2 = 8.04$ ns (39.96 %) |
| 7 | 100 | $\tau_1 = 0.04$ ns (71.15 %) $\tau_2 = 7.80$ ns (28.35 %) |

Table S5. Emission lifetime of **D1:N1** (1:1) in acetonitrile with increasing % of water ($C = 0.1$ mM, $\lambda_{\text{mon}} = 530$ nm, $\lambda_{\text{ex}} = 374$ nm).

| Sr. No | % of water | Lifetime |
|--------|------------|---|
| 1 | 0 | $\tau_1 = 0.087$ ns (33.66 %) $\tau_2 = 7.53$ ns (66.34 %) |
| 2 | 20 | $\tau_1 = 0.062$ ns (38.42 %) $\tau_2 = 7.76$ ns (61.58 %) |
| 3 | 40 | $\tau_1 = 0.057$ ns (48.73 %) $\tau_2 = 6.26$ ns (51.27 %) |
| 4 | 60 | $\tau_1 = 0.052$ ns (63.12 %) $\tau_2 = 5.87$ ns (36.88 %) |
| 5 | 80 | $\tau_1 = 0.04$ ns (67.16 %) $\tau_2 = 5.79$ ns (32.84 %) |
| 6 | 90 | $\tau_1 = 0.051$ ns (58.78 %) $\tau_2 = 5.89$ ns (41.22 %) |
| 7 | 100 | $\tau_1 = 0.046$ ns (44.18 %) $\tau_2 = 8.48$ ns (55.82 %) |

Table S6. Emission lifetime of **EL** ($\lambda_{\text{mon}} = 390$ nm, $\lambda_{\text{ex}} = 374$ nm).

| Sr. No | D1:N1 | Lifetime |
|--------|---------|---|
| 1 | 1:0 | $\tau_1 = 0.12$ ns (35.74 %) $\tau_2 = 8.67$ ns (64.26 %) |
| 2 | 1:0.025 | $\tau_1 = 0.046$ ns (56.77 %) $\tau_2 = 8.23$ ns (43.23 %) |
| 3 | 1:0.05 | $\tau_1 = 0.022$ ns (69.17 %) $\tau_2 = 8.19$ ns (30.83 %) |
| 4 | 1:0.075 | $\tau_1 = 0.027$ ns (67.65 %) $\tau_2 = 8.13$ ns (32.35 %) |
| 5 | 1:0.1 | $\tau_1 = 0.014$ ns (89.38 %) $\tau_2 = 7.69$ ns (10.62 %) |

Table S7. Emission lifetime of **EL** ($\lambda_{\text{mon}} = 530$ nm, $\lambda_{\text{ex}} = 374$ nm).

| Sr. No | D1:N1 | Lifetime |
|---------------|--------------|-----------------------------|
| 1 | 1:0 | $\tau_1 = 0.067$ ns (100 %) |
| 2 | 1:0.025 | $\tau_1 = 14.20$ ns (100 %) |
| 3 | 1:0.05 | $\tau_1 = 14.77$ ns (100 %) |
| 4 | 1:0.075 | $\tau_1 = 14.90$ ns (100 %) |
| 5 | 1:0.1 | $\tau_1 = 14.96$ ns (100 %) |

Table S8. Emission lifetime of **EL** ($\lambda_{\text{mon}} = 530$ nm, $\lambda_{\text{ex}} = 374$ nm).

| Sr. No | Sample (D1:N1) | Lifetime |
|---------------|-----------------------|--|
| 1 | 1:0 | $\tau_1 = 0.067$ ns (100 %) |
| 2 | 1:0.1 | $\tau_1 = 14.96$ ns (100 %) |
| 3 | 1:0.5 | $\tau_1 = 0.071$ ns (23.44 %) $\tau_2 = 15.21$ ns (76.56 %) |
| 4 | 1:1 | $\tau_1 = 0.21$ ns (8.50 %) $\tau_2 = 15.58$ ns (91.50 %) |
| 5 | 1:2 | $\tau_1 = 0.54$ ns (8.05 %) $\tau_2 = 15.90$ ns (91.95 %) |

Table S9. The luminescence quantum yield of **D1**, **N1** and **EL**.

| Sr. No. | Sample | QY of monomers (%) | QY of EL (%) |
|----------------|------------------------|---------------------------|---------------------|
| 1 | D1 | 19.09 | - |
| 2 | N1 | 10.05 | - |
| 3 | D1:N1 (1:0.001) | 10.96 | 0.46 |
| 4 | D1:N1 (1:0.005) | 6.93 | 0.87 |
| 5 | D1:N1 (1:0.01) | 6.43 | 1.03 |
| 6 | D1:N1 (1:0.05) | 2.74 | 1.69 |
| 7 | D1:N1 (1:0.1) | 0.56 | 2.49 |
| 8 | D1:N1 (1:0.5) | - | 2.51 |
| 9 | D1:N1 (1:1) | - | 1.98 |
| 10 | D1:N1 (1:1.5) | - | 1.63 |

Table S10. Emission lifetime of **EL** with different acceptors ($\lambda_{\text{mon}} = 530 \text{ nm}$, $\lambda_{\text{ex}} = 374 \text{ nm}$).

| Sr. No | Sample | Lifetime |
|--------|---------------|---|
| 1 | EL | $\tau_1 = 1.63 \text{ ns (17.51 \%)}$ $\tau_2 = 15.42 \text{ ns (82.49 \%)}$ |
| 2 | EL+RDX | $\tau_1 = 1.51 \text{ ns (12.68 \%)}$ $\tau_2 = 15.41 \text{ ns (87.32 \%)}$ |
| 3 | EL+AQ | $\tau_1 = 1.24 \text{ ns (17.84 \%)}$ $\tau_2 = 14.53 \text{ ns (82.16 \%)}$ |
| 4 | EL+NP | $\tau_1 = 1.87 \text{ ns (41.05 \%)}$ $\tau_2 = 12.12 \text{ ns (58.95 \%)}$ |
| 5 | EL+NB | $\tau_1 = 1.69 \text{ ns (24.69 \%)}$ $\tau_2 = 9.84 \text{ ns (75.31 \%)}$ |
| 6 | EL+NT | $\tau_1 = 2.04 \text{ ns (18.66 \%)}$ $\tau_2 = 13.15 \text{ ns (81.34 \%)}$ |
| 7 | EL+DNT | $\tau_1 = 2.01 \text{ ns (24.39 \%)}$ $\tau_2 = 13.12 \text{ ns (75.21 \%)}$ |
| 8 | EL+TNT | $\tau_1 = 0.098 \text{ ns (68.32 \%)}$ $\tau_2 = 3.11 \text{ ns (31.68 \%)}$ |

Table S11. Emission lifetime of **EL** with different weight percent of TNT acceptors ($\lambda_{\text{mon}} = 530 \text{ nm}$, $\lambda_{\text{ex}} = 374 \text{ nm}$).

| Sr. No | Sample | Lifetime |
|--------|-----------------------|---|
| 1 | EL | $\tau_1 = 1.63 \text{ ns (17.51 \%)}$ $\tau_2 = 15.42 \text{ ns (82.49 \%)}$ |
| 2 | EL+ 1 Wt % TNT | $\tau_1 = 0.11 \text{ ns (57.22 \%)}$ $\tau_2 = 7.71 \text{ ns (42.78 \%)}$ |
| 3 | EL+10 Wt % TNT | $\tau_1 = 0.098 \text{ ns (68.32 \%)}$ $\tau_2 = 3.11 \text{ ns (31.68 \%)}$ |

Table S12. HOMO, LUMO, and HOMO-LUMO energy gap and π - π stacking interaction of D1, N1, EL, and EL+TNT.

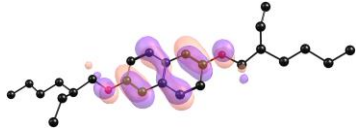



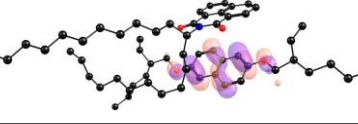
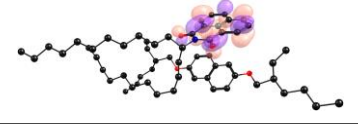
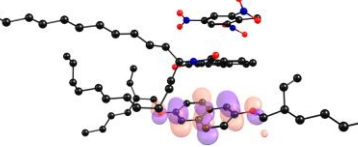

| Molecule | HOMO | LUMO | HOMO-LUMO energy gap (eV) |
|----------|--|---|---------------------------|
| D1 |  |  | 4.09 |
| N1 |  |  | 3.96 |
| EL |  |  | 2.53 |
| EL+TNT |  |  | 1.55 |

Table S13. HOMO, LUMO, and HOMO-LUMO energy gap and π - π stacking interaction of D2, N2, D2:N2, and D2:N2+TNT.

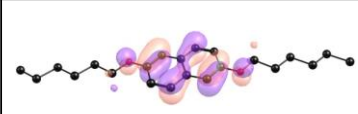
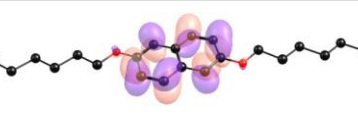
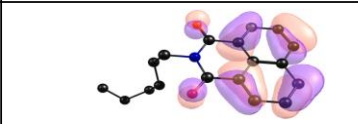
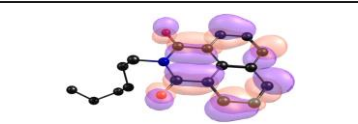
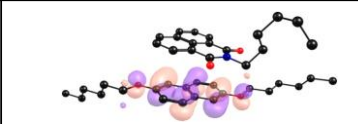
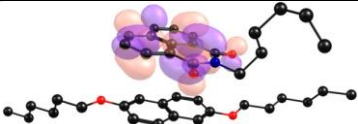
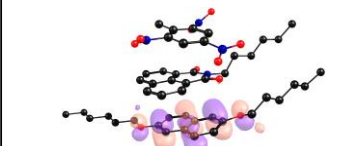

| Molecule | HOMO | LUMO | HOMO-LUMO energy gap (eV) |
|-----------|---|--|---------------------------|
| D2 |  |  | 4.07 |
| N2 |  |  | 3.96 |
| D2:N2 |  |  | 2.64 |
| D2:N2+TNT |  |  | 1.77 |

Table S14. Binding energy calculation, HOMO-LUMO gap, and π - π stacking interaction of EL, D1, and N1 with different nitroaromatic acceptors.

| Complex | ΔE (kcal/mol) | HOMO-LUMO gap (eV) | π-π stacking distance (Å) |
|----------------|---|---------------------------|--|
| EL+TNT | -14.0 | 1.55 | 3.64 |
| EL +DNT | -11.2 | 2.03 | 3.67 |
| EL +NT | -15.7 | 2.43 | 3.72 |
| EL +NB | -15.4 | 2.34 | 3.62 |
| EL +NP | -11.1 | 2.39 | 3.91 |
| EL +Tol | -9.6 | 2.56 | 3.97 |
| EL +RDX | -12.3 | 2.17 | - |
| EL +AQ | -13.3 | 2.05 | 3.92 |
| <hr/> | | | |
| Complex | ΔE (kcal/mol) | HOMO-LUMO gap (eV) | π-π stacking distance (Å) |
| D1+TNT | -18.1 | 2.13 | 3.21 |
| D1 +DNT | -16.1 | 2.35 | 3.23 |
| D1+NT | -18.0 | 2.73 | 3.94 |
| D1 +NB | -16.0 | 2.63 | 3.34 |
| D1 +NP | -13.5 | 2.99 | 3.78 |
| D1 +Tol | -7.0 | 4.05 | 3.66 |
| D1+RDX | -17.3 | 3.16 | - |
| D1 +AQ | -13.3 | 2.27 | 3.25 |
| <hr/> | | | |
| Complex | ΔE (kcal/mol) | HOMO-LUMO gap (eV) | π-π stacking distance (Å) |
| N1+TNT | -15.1 | 3.17 | 3.47 |

| | | | |
|----------------|-------|------|------|
| N1 +DNT | -14.7 | 3.51 | 3.65 |
| N1+NT | -19.0 | 3.85 | 3.80 |
| N1+NB | -16.8 | 3.73 | 3.52 |
| N1+NP | -14.1 | 3.57 | 3.66 |
| N1+Tol | -9.9 | 3.80 | 3.82 |
| N1+RDX | -13.7 | 3.89 | - |
| N1+AQ | -13.9 | 3.95 | 3.54 |

References

- S1. R. Ahlrichs, M. Bar, M. Häser, H. Horn and C. Kölmel, *Chem. Phys. Lett.*, **1989**, *162*, 165–169.
- S2. J. P. Perdew, K. Burke and M. Ernzerhof, *Phys. Rev. Lett.*, **1996**, *77*, 3865–3868.
- S3. S. Ansgar, H. Christian and A. Reinhart, *J. Chem. Phys.*, **1994**, *100*, 5829–5835.
- S4. K. Eichkorn, O. Treutler, H. Öhm, M. Häser and R. Ahlrichs, *Chem. Phys. Lett.*, **1995**, *240*, 283–289.
- S5. M. Sierka, A. Hogekamp, R. Ahlrichs, *J. Chem. Phys.*, **2003**, *118*, 9136-9148.
- S6. Gaussian 09, Revision E.01; M. J. Frisch, G. W. Trucks, H. B. Schlegel, G. E. Scuseria, M. A. Robb, J. R. Cheeseman, G. Scalmani, V. Barone, B. Mennucci, G. A. Petersson, H. Nakatsuji, M. Caricato, X. Li, H. P. Hratchian, A. F. Izmaylov, J. Bloino, G. Zheng, J. L. Sonnenberg, M. Hada, M. Ehara, K. Toyota, R. Fukuda, J. Hasegawa, M. Ishida, T. Nakajima, Y. Honda, O. Kitao, H. Nakai, T. Vreven, J. A. Montgomery, Jr., J. E. Peralta, F. Ogliaro, M. Bearpark, J. J. E. Heyd, K. N. B. Kudin, V. N. Staroverov, R. Kobayashi, J. K. Raghavachari, A. Rendell, J. C. Burant, S. S. Iyengar, J. Tomasi, M. Cossi, N. Rega, J. M. Millam, M. Klene, J. E. Knox, J. B. Cross, V. Bakken, C. Adamo, J. Jaramillo, R. Gomperts, R. E. Stratmann, O. Yazyev, A. J. Austin, R. Cammi, C. Pomelli, J. W. Ochterski, R. L. Martin, K. Morokuma, V. G. Zakrzewski, G. A. Voth, P. Salvador, J. J. Dannenberg, S. Dapprich, A. D. Daniels, Ö. Farkas, J. B. Foresman, J. V. Ortiz, J. Cioslowski, D. J. Fox, Gaussian, Inc., Wallingford CT, **2009**.
- S7. Wakchaure, V. C.; Pillai, L. V.; Goudappagouda, Ranjeesh, K. C.; Chakrabarty, S.; Ravindranathan, S.; Rajamohanam, P. R. Babu, S. S., *Chem. Commun.*, **2019**, *55*, 9371-9374.
- S8. Wescott, L. D.; Mattern, D. L., *J. Org. Chem.* **2003**, *68*, 10058–10066.
- S9. Goudappagouda, Manthanath, A.; Wakchaure, V. C.; Ranjeesh, K. C.; Das, T.; Vanka, K.; Nakanishi, T.; Babu, S. S., *Angew. Chem. Int. Ed.*, **2019**, *58*, 2284-2288.